NASA CONTRACTOR REPORT

NASA CR-1670

BEHAVIOR OF FLUIDS IN THE VICINITY OF THE CRITICAL POINT

by K. Fritsch and E. F. Carome

Prepared by
JOHN CARROLL UNIVERSITY
University Heights, Ohio
for

NATIONAL AERONAUTICS AND SPACE ADMINISTRATION • WASHINGTON, D. C. • SEPTEMBER 1970

Call no.

1. Report No.	2. Government Accession No.	3. Recipient's Catalog No.
NASA CR-1670		

4. Title and Subtitle	5. Report Date
BEHAVIOR OF FLUIDS IN THE VICINITY OF THE CRITICAL POINT	September 1970
	6. Performing Organization Code

7. Author(s)	8. Performing Organization Report No.
K. Fritsch and E. F. Carome	None

9. Performing Organization Name and Address	10. Work Unit No.
John Carroll University, Dept. of Physics, University Heights, Ohio	NGR 36-006-002
	11. Contract or Grant No.
	13. Type of Report and Period Covered: Contractor Report

12. Sponsoring Agency Name and Address	14. Sponsoring Agency Code
National Aeronautics and Space Administration, Washington, D. C. 20546	

15. Supplementary Notes

16. Abstract

Results of recent analyses of critical point behavior of single component fluids are presented. Acoustical and optical techniques for studying such behavior are discussed and experimental systems developed for this work are described. Results of sound velocity and absorption measurements in CO_2 and SF_6 in the kilohertz and megahertz range and limited light scattering measurements in SF_6 are presented. Low frequency sound velocity measurements in CO_2 indicate that the adiabatic compressibility and the specific heat at constant volume may diverge logarithmically as the critical point is approached along the critical isochore.

17. Key Words (Suggested by Author(s))	18. Distribution Statement
Critical point Ultrasonics Light scattering	Unclassified - unlimited

19. Security Classif. (of this report)	20. Security Classif. (of this page)	21. No. of Pages	22. Price*
Unclassified	Unclassified	75	$3.00

*For sale by the Clearinghouse for Federal Scientific and Technical Information
Springfield, Virginia 22151

FOREWORD

The work described herein was done in the laboratories of the Department of Physics at John Carroll University under NASA grant NGR 36-006-002 with Mr. William J. Masica, Spacecraft Technology Division, NASA Lewis Research Center, as Project Manager.

CONTENTS

CONTENTS cont.

SUMMARY

The thermodynamic behavior of single component fluids in the vicinity of the gas-liquid critical point is briefly reviewed. It is pointed out that classical theories, based on the assumption that there exists an analytic equation of state, fail to account satisfactorily for experimental results in the critical region. Some predictions of recent theoretical studies are considered and various critical point exponents are introduced. These currently are employed to describe observed divergences of the compressibilities, specific heats and other physical parameters, as the critical point is approached.

Acoustical and optical techniques for determining the properties of fluids are discussed and several systems developed for such work during the present experimental study of critical point phenomena are described in detail. These include systems for the measurement of the velocity of sound in the low kilohertz range and for the velocity and absorption of sound in the megahertz range, as well as those developed for studies of the Brillouin components in the scattered light spectrum. Precise temperature control and fluid cell filling procedures employed in the present study also are described.

Results of extensive velocity of sound measurements in carbon dioxide are presented. A resonant cavity technique for isochoric measurements at frequencies in the vicinity of one kilohertz has been employed and the values of velocity obtained are substantially lower than those reported by other workers. Analysis of the data yields information on the behavior of the adiabatic compressibility and the constant volume specific heat. It has been concluded that for CO_2 the adiabatic compressibility may diverge logarithmically as the critical temperature is approached from above along the critical isochore. In addition, the specific heat at constant volume may also diverge logarithmically.

Experimental data obtained in low frequency acoustic velocity measurements in sulfur hexafluoride and megahertz acoustic measurements of velocity and sound absorption in CO_2 and SF_6 also are presented, together with results obtained in preliminary light scattering studies of these fluids in the critical region.

I. INTRODUCTION

When a fluid exists as a two phase system consisting of a liquid phase and a vapor phase in equilibrium under ordinary laboratory conditions, it is usually easy to distinguish one phase from the other, since there may be large differences in the values of most physical properties such as density, specific heat, compressibility, viscosity, heat conductivity, optical refractive index, and so forth. As the temperature is increased, however, the differences between the properties of the two phases become less and less pronounced. Finally, in the vicinity of the critical point the differences vanish and there is only a single gaseous phase above the critical temperature.

Visual observations of the behavior of fluids in the vicinity of the critical point and determinations of their thermodynamic properties in this region have been made for more than a hundred years. The critical temperature of carbon dioxide was discovered by Andrews in 1869 [1]. Until quite recently it was assumed that the subject of critical point behavior was well understood. Small discrepancies between theory and experiment were attributed to experimental difficulties. However, precise measurements carried out during the past decade have revealed several obvious differences between theory and experiment, and it now seems clear that classical theories relating to the behavior of materials near their critical point are totally inadequate to explain observed effects. Efforts are being made by many workers to develop new theories, some related to the Ising model [2], which in two dimensional form was successfully applied to predict nonclassical behavior, and others which have lead to various scaling-law equations of state [3-5].

On the experimental side, many groups are concentrating their efforts on determining as accurately as possible the properties of fluids in the critical region. Approximately three years ago we decided to join in this effort, since it forms a direct extension of research that has been in progress for more than ten years in the Department of Physics of John Carroll University. In this work we are applying several techniques that we had developed for determining equilibrium and transport properties of liquids. These include acoustic velocity and absorption methods and Rayleigh and Brillouin light scattering techniques.

In the first half of this report we summarize current knowledge of critical phenomena as far as it applies to the experiments carried out by our group. The second half of the report contains a detailed discussion of the experimental techniques we have employed and the results we have obtained during the past two years in studies of the properties of carbon dioxide and sulfur hexafluoride in the critical region. We then compare our data with those of other workers and with the predictions of recent theoretical work. For more information on critical point phenomena the interested reader is directed to detailed theoretical papers on equilibrium properties by Fisher [6] and by Kadanoff et al [5]. A report of the proceedings of a conference on critical phenomena held in 1965 [7] provides a summary of experimental work performed prior to that date and Heller [8] presents an excellent review of recent work.

II. THERMODYNAMICS OF THE CRITICAL POINT

2.1 Definition of the Critical Point

It is usually assumed that the behavior of a fluid may be expressed by an equation of state of the form

$$f(P,V,T) = 0 \tag{1}$$

where f is some well behaved function of the pressure P, the specific volume V, and the absolute temperature T. Any state of the fluid can therefore be represented as a point on the surface of state in the three dimensional PVT space. A sketch of a portion of this PVT surface for a typical fluid is shown in Fig. 1, where the single phase regions of liquid, vapor, or gas, and the two phase region are so labeled. Points on the latter portion of the PVT surface, which is enclosed by the coexistence curve C'CC", represent those states of the fluid where liquid and vapor coexist in equilibrium at the pressure, temperature, and total specific volume defining the point. By considering the intersections of the surface of state with planes perpendicular to the T, P, or V axis, respectively, the isotherms of P versus V, the isobars of T versus V, and the isochores of P versus T may be obtained. These are shown in Fig. 2.

The point C in Fig. 1 and its projections indicated in Fig. 2 represent the critical point state of the fluid which has been defined in several ways:

(a) It is that state of the fluid where the coexisting liquid and vapor specific volumes, and therefore the corresponding densities, become equal, i.e. it is the uppermost point, in temperature and pressure, on the coexistence curve. The critical temperature T_c, therefore, is the highest temperature at which the two distinct phases of liquid and vapor may be present simultaneously.

(b) Referring to Fig. 2a, the isotherm for $T = T_c$ is usually assumed to have an inflection point at $V = V_c$, so that

$$(\partial P/\partial V)_{T_c,V_c} = 0 = (\partial^2 P/\partial V^2)_{T_c,V_c} \tag{2}$$

Both of these have been used as definitions of the critical state.

It should be pointed out that theoretical questions have been raised recently concerning whether conditions (a) and (b) define the same state. In addition, experimental data seem to indicate that higher order derivatives of the isotherms may also vanish at the critical point. For the present, however, we shall assume that (a) and (b) define a single state, i.e. the critical point. In Table I we have summarized available experimental data on four fluids studied extensively by researchers interested in critical point phenomena.

The fact that the liquid and vapor densities become equal and that the derivatives appearing in Eq. (2) are zero at the critical point leads to much of the intriguing behavior that is observed as a fluid sample is brought into

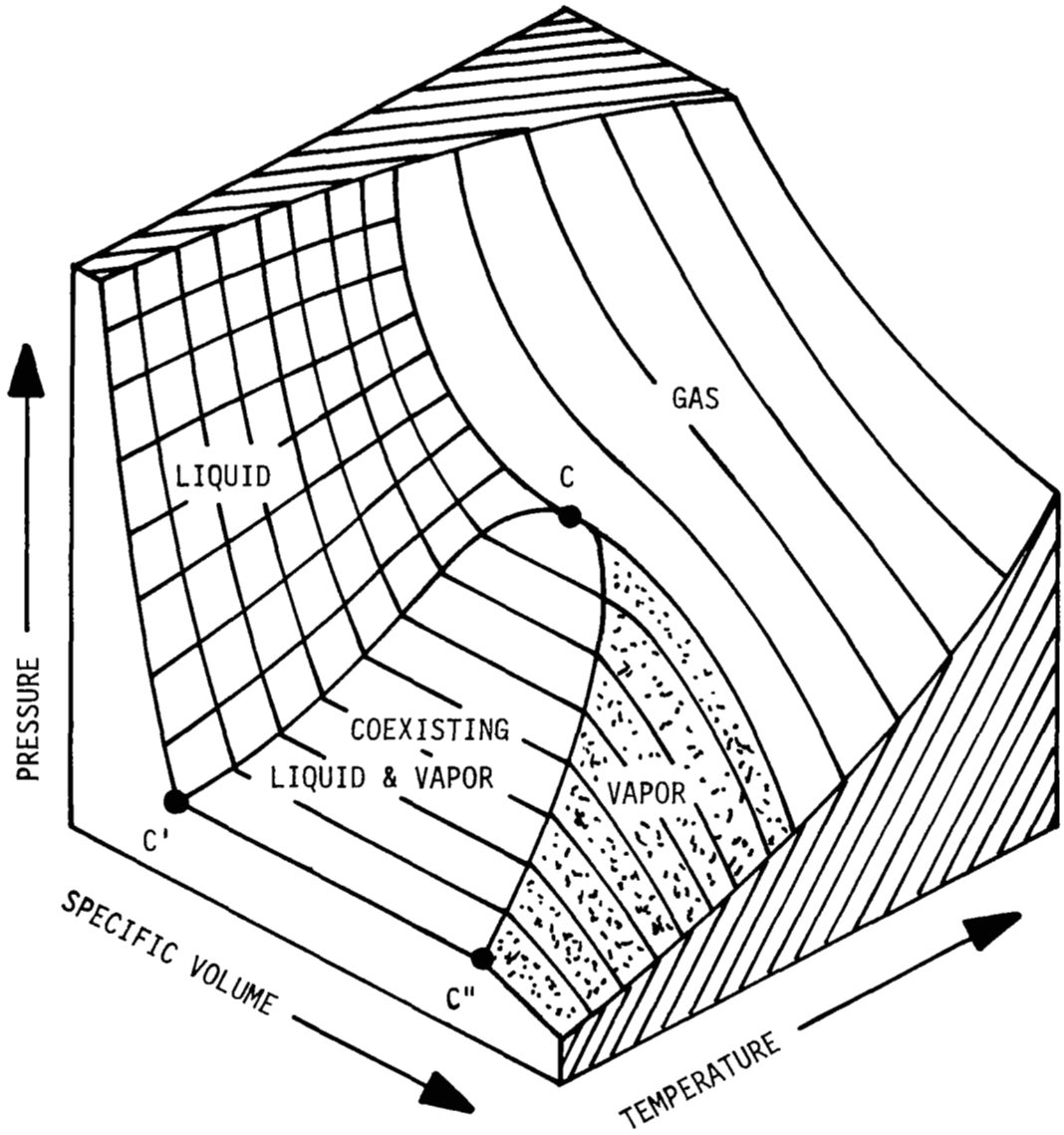

FIG. 1. SURFACE OF STATE IN THE VICINITY OF THE CRITICAL POINT.

FIG. 2a
PRESSURE-VOLUME
DIAGRAM

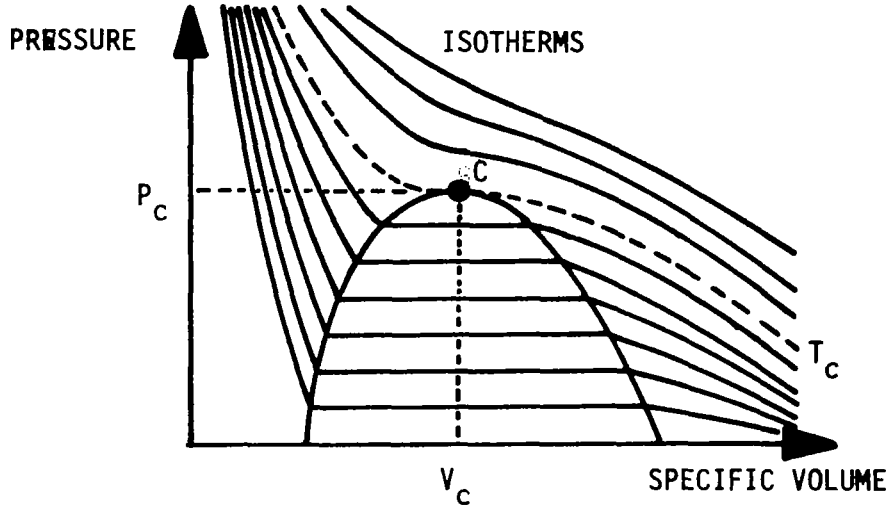

FIG. 2b
PRESSURE-TEMPERATURE
DIAGRAM

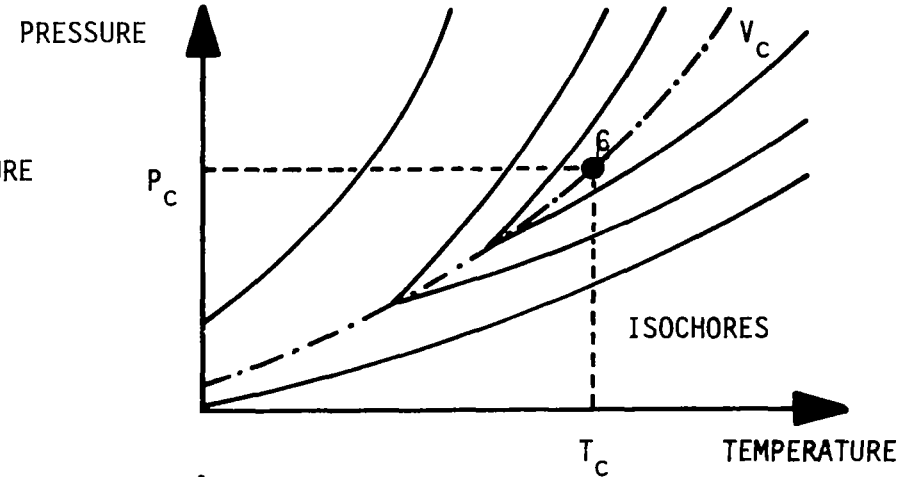

FIG. 2c
TEMPERATURE-VOLUME
DIAGRAM

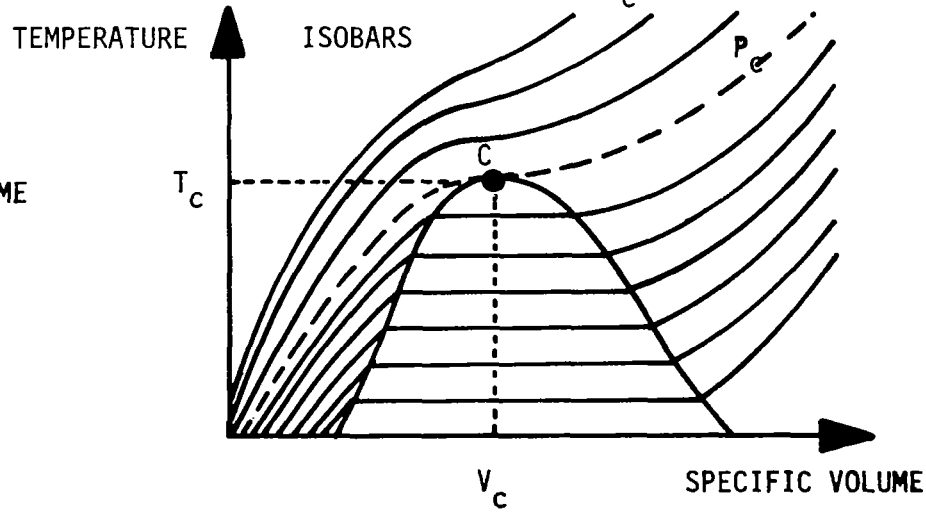

FIG. 2. PROJECTIONS OF THE SURFACE OF STATE.

TABLE I EXPERIMENTAL CRITICAL PARAMETERS

Fluid	P_c (atm)	T_c (°C)	T_c (K)	ρ_c (g/cm^3)	v_c (cm^3/g)	Reference
X_e	57.6	16.59	289.75	1.11	0.905	[5] p. 419
Ar	48.3	-122.29	150.71	0.533	0.533	[5] p. 419
CO_2	72.8	31.04	304.20	0.464	2.14	[5] p. 419
SF_6	37.8	45.6	318.8	0.73	1.36	[51]p. 2257

the vicinity of this state. We wish to consider first the general behavior of some thermodynamic quantities that may be deduced from the topology of observed PVT surfaces.

2.2 Infinite Thermodynamic Derivatives in the Two Phase Region

Before considering the behavior of a fluid in the vicinity of the critical point it is useful to discuss several obvious "anomalies" that occur in the two phase region. As indicated in Fig. 2a, the isotherms have zero slope in the coexistence region. Thus, the isothermal compressibility κ_T, in terms of V or the mass density ρ, given by

$$\kappa_T = -V^{-1}(\partial V/\partial P)_T = \rho^{-1}(\partial \rho/\partial P)_T \tag{3}$$

is infinite for a fluid sample in this region. This merely means that if the volume of a liquid-vapor sample is changed at constant temperature the pressure does not change as long as both phases are present. As the volume is increased, some liquid evaporates, thus producing the required increase in volume, since the specific volume is larger for the vapor than for the liquid.

From the behavior of the fluid during this same process, i.e. expansion in the two phase region which takes place at constant temperature and at constant pressure, it is obvious that the thermal expansion coefficient α_p, defined by

$$\alpha_p = V^{-1}(\partial V/\partial T)_p = -\rho^{-1}(\partial \rho/\partial T)_p \tag{4}$$

is also infinite in the two phase region. Also, since at constant temperature an amount of heat dQ must be added to vaporize some of the liquid in a sample of total mass m, the specific heat at constant pressure C_p, defined by

$$C_p = (dQ/dT)_p/m \tag{5}$$

is infinite in the two phase region.

On the other hand, except in the immediate vicinity of the critical point, when heat is added to a fluid at constant volume in the two phase region, the temperature increases. Therefore, the specific heat at constant volume C_v, given by

$$C_v = (dQ/dT)_V/m \tag{6}$$

is finite. Thus, the ratio of specific heats γ^*, defined as

$$\gamma^* = C_p/C_v \tag{7}$$

is infinite over much of the two phase region. Experimentally however, C_v is observed to become large in the immediate vicinity of the critical point and there is evidence that along the critical isochore C_v versus T diverges weakly as T approaches T_c [9-13].

2.3 Infinite Thermodynamic Derivatives in the One Phase Region

In the previous section we pointed out that several thermodynamic derivatives for a simple fluid are infinite in the two phase region. This behavior is due to the phase transition, i.e. evaporation of liquid or condensation of vapor, and is not due to any intrinsic property of either of the separate phases. Of more fundamental interest is the occurrence of infinite derivatives, again in the vicinity of the critical point, but in the one phase region. We first discussed the two phase infinities, however, because we feel their occurrence is easily understood, and in some sense may help explain similar behavior in the one phase regions.

Consider, for example, the behavior of a fluid in the gaseous region. As the critical temperature T_c is approached from above, as indicated earlier in Fig. 2a, the slope of the isotherms, representing P as a function of V, approaches zero in the critical region, where the density $\rho \simeq \rho_c$, and we may write

$$\lim[T\to T_c,\rho\to\rho_c]\ \kappa_T \to \infty\ ;\ [T>T_c] \tag{8}$$

This same behavior of the isotherms leads one to conclude that the specific heat C_p must also diverge, i.e.

$$\lim[T\to T_c,\rho\to\rho_c]\ C_p \to \infty\ ;\ [T>T_c] \tag{9}$$

Also, since the isobars behave similarly, we have

$$\lim[T\to T_c,\rho\to\rho_c]\ \alpha_p \to \infty\ ;\ [T>T_c] \tag{10}$$

Unfortunately, the occurrence of the observed divergence of C_v may not be deduced in such a direct manner from the topology of the PVT surface [14] and we shall defer considering its behavior.

Of major interest is the exact manner in which the various thermodynamic derivatives diverge as the critical region is approached, since this may provide information required to develop a satisfactory theory of dense fluids. This is the ultimate goal of much of the experimental work on critical point behavior currently in progress in many laboratories. It forms the basis of the acoustic and light scattering research initiated by the authors of this report and pertinent results are presented in later sections.

III. CLASSICAL VERSUS NONCLASSICAL BEHAVIOR

So called classical theories of critical point behavior of simple fluids begin with the assumption that the Helmholtz free energy F is analytic in the vicinity of the critical point, i.e. that F may be expanded as a Taylor series in temperature and specific volume about the critical point. Such an equation of state was proposed by van der Waals in 1873 to explain the behavior of the isotherms of CO_2 near the critical point. Combined with Maxwell's equal area construction, this equation has been used quite successfully to explain at least qualitatively much of the observed behavior of fluids. With some modifications, other analytic equations of state may be obtained which yield good quantitative agreement with experiment over a large portion of the gaseous region.

In recent years, however, there has been a growing realization that experimental data on critical point behavior appears to be inconsistent with the predictions of any theory based on the assumption that F is analytic throughout the critical region. This point may be illustrated by considering the shape of the coexistence curve. In the following figure, the projection of the coexistence curve on the temperature-density plane is sketched.

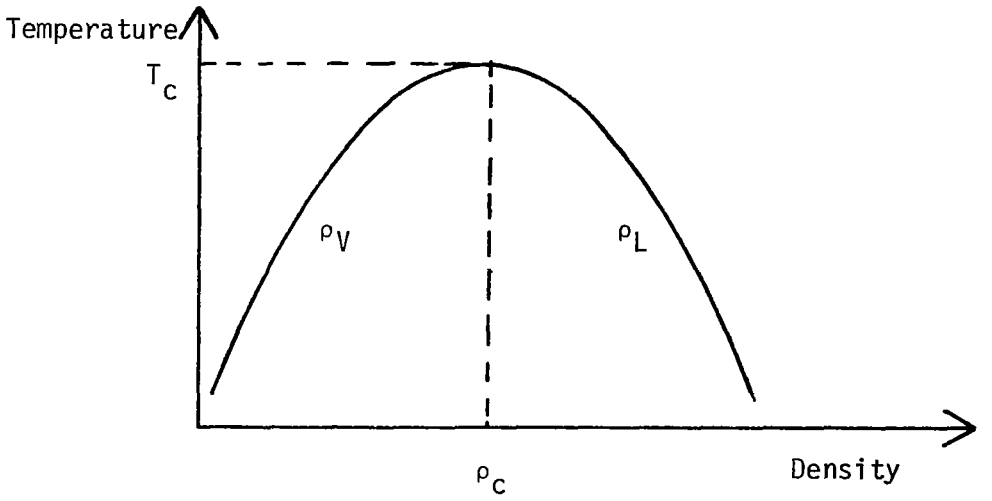

The density ρ rather than the specific volume V is frequently employed, since a plot of T versus ρ yields a more symmetric curve than that of T versus V. A fluid described by the van der Waals equation of state leads to a coexistence curve satisfying the expression

$$\rho_L - \rho_V \sim (T_c - T)^{1/2}; \quad [T<T_c] \tag{11}$$

where ρ_L and ρ_V are the densities of coexisting liquid and vapor, respectively. More generally, for <u>any</u> classical equation of state,

$$\rho_L - \rho_V \sim (T_c - T)^{\beta} \quad ; \quad [T<T_c] \tag{12}$$

where $\beta = 1/2, 1/4, \ldots, 1/(2n)$ with n being a nonzero, positive integer, depending on the order of the first nonvanishing derivative of F with respect to V. Experimentally, however, very careful studies of the behavior of a number of fluids [15-17] have shown that the proportionality indicated in Eq. (12) applies but with the exponent $\beta \simeq 0.33$ to 0.40, i.e. not the reciprocal of an even integer. This result is typical of the type of differences that are noted between the predictions of classical theories and experimental results.

IV. CRITICAL EXPONENTS

As pointed out in the previous section, experimental results appear to indicate that some exponents characterizing critical point behavior, such as β in the expression shown in Eq. (12), may differ substantially from the values predicted by analytic equations of state. It has therefore become of interest to study in great detail, both theoretically and experimentally, these so-called critical exponents. These describe the asympotic behavior of various thermodynamic quantities as the critical point is approached along different paths on the surface of state.

As indicated by Fisher [6], a critical point exponent may be defined as follows: Consider a thermodynamic quantity f that is a function of a parameter x. Assume x goes to zero as the critical point is approached from a given direction along a particular path. Then, if the relation

$$\lim_{x \to 0} \frac{\ln[f(x)]}{\ln[x]} = \pi \tag{13}$$

is satisfied, the quantity π is defined as a critical exponent for this path. Thus we may write

$$f(x) \sim x^{\pi} \text{ as } x \to 0 \tag{14}$$

i.e. f(x) behaves as x^{π} asymptotically, as the critical point is approached along the defined path.

The quantity x may be the relative temperature difference ε defined by

$$\varepsilon = \frac{T-T_c}{T_c} \tag{15}$$

or in other instances $(\rho-\rho_c)/\rho_c$, $(P-P_c)/P_c$ or some similar parameter.

The defining expression for the critical exponents given in Eq. (13) does not exclude the existence of a logarithmic factor, i.e.

$$f(x) \sim x^{\pi} |\ln x| \tag{16}$$

since in the limit as $x \to 0$, f(x) may be set equal to x^{π} for $\pi \neq 0$. In addition, if $\pi = 0$, there are several possibilities: either f(x) may diverge as $|\ln x|$, or f(0) may be finite with f(x) being either continuous or discontinuous as x passes through zero.

Without extending the discussion to more complicated possibilities, it should be evident that difficulties may arise when one attempts to deduce unambiguously a particular form for f(x) from experimental data. This is particularly so since the experimental data is usually limited to a small temperature range. For example, it may be shown that in the limit as x goes

to zero, a small algebraic power law dependence (e.g. $\pi \simeq -0.2$ in Eq. (14)) is indistinguishable from logarithmic behavior over small ranges of x.

This formalism, however, as pointed out by Kadanoff and others [5], does allow one to define the critical region in a meaningful way. Referring to Eq. (13), it is that region on the PVT surface where thermodynamic functions f(x) approach a specific behavior, i.e. a fixed exponent π, as the pertinent parameter x approaches zero.

Since in this report we are interested in the behavior of simple fluids near the liquid-vapor critical point, we will now define several of the appropriate critical point exponents for this type of system. Each applies to a specific path on the PVT surface.

a) We have already introduced the exponent β used to describe the density difference $\rho_L - \rho_V$ between coexisting liquid and vapor as the critical temperature is approached from below:

$$\rho_L - \rho_V \sim (-\varepsilon)^{\beta} \quad [\text{coexistence curve}; \varepsilon < 0) \tag{17}$$

b) The isothermal compressibility κ_T of the gaseous phase diverges as $\varepsilon^{-\gamma}$ where γ is positive, as the critical temperature is approached from above along the critical isochore:

$$\kappa_T \sim \varepsilon^{-\gamma} \quad [\text{critical isochore: } \rho = \rho_c; \varepsilon > 0] \tag{18}$$

c) It is possible to define exponents describing the behavior of the isothermal compressibilities κ_{TL} and κ_{TV} of the liquid and of the vapor phase, respectively. It is found that these two compressibilities diverge in the same manner as T approaches T_c. Thus a single exponent γ' is sufficient to describe their behavior:

$$\kappa_{T_{L,V}} \sim (-\varepsilon)^{-\gamma'} \quad [\text{coexistence curve}; \varepsilon < 0] \tag{19}$$

d) The behavior of the critical isotherm $P = P(\rho)_{T = T_c}$ in the critical region may be defined by introducing an exponent δ:

$$|P - P_c| \sim |\rho - \rho_c|^{\delta} \quad [\text{critical isotherm: } \varepsilon = 0] \tag{20}$$

e) The final critical exponents to be introduced here describe the behavior of the specific heat at constant volume C_V. Along the critical isochore, as T approaches T_c from above, C_V diverges and we write

$$C_V \sim \varepsilon^{-\alpha} \quad [\text{critical isochore: } \rho = \rho_c; \varepsilon > 0] \tag{21}$$

f) The specific heats of the liquid and of the vapor phase along the coexistence curve may be considered separately. As with the isothermal compressibilities, their behavior in the critical region is the same and it is possible to define a single exponent α':

$$C_{V_{L,V}} \sim (-\varepsilon)^{-\alpha'} \quad [\text{coexistence curve};\varepsilon<0] \tag{22}$$

g) A third exponent α'' is very often determined from measurements of C_V on a two phase sample with mean density of ρ_c, i.e. along the extension of the critical isochore below T_c

$$C_V \sim (-\varepsilon)^{-\alpha''} \quad (\rho = \rho_c,\ \varepsilon< 0) \tag{23}$$

It may be shown that asymptotically $\kappa_S=\kappa_T/\gamma^*$ diverges as C_V and C_p diverges as κ_T.

In Table II the values for these exponents, determined experimentally by various workers for several fluids, are summarized. The experimental values are compared with the exponents predicted using classical theories as well as those obtained from calculations based on the three dimensional Ising model, i.e. a nonanalytic approach. It should be pointed out that several rigorous exponent inequalities have been derived which relate the critical point exponents [18,19]. The number of independent exponents necessary to describe equilibrium quantities has not been established, but an attempt has been made to relate all equilibrium critical exponents to two basic ones [18].

TABLE II CRITICAL EXPONENTS

Exponent	Experiment	Classical Theory	3 Dimensional Ising Model
α	$\gtrsim 0$;(ln)	0;(discontinuous)	0.125
α'	$\simeq 0$;(ln)	0;(discontinuous)	0.0625
β	$\simeq 0.35$	0.5	0.312
γ	$\gtrsim 1.2$	1.0	1.25
γ'	$\gtrsim 1.2$	1.0	1.312
δ	$\simeq 4.3$	3.0	5.2

The experimental values are average values for a number of single component fluids. For the experimental values in specific fluids, see references [5,6,8].

V. ACOUSTIC MEASUREMENTS OF CRITICAL POINT BEHAVIOR

We have pointed out before that one of the objectives of critical point measurements is to determine the critical exponents of a number of thermodynamic quantities. A few of these may be obtained by thermodynamic measurements, such as direct specific heat measurements or isothermal compressibility measurements. As we will show in the following sections, both acoustic and light scattering methods supply a wealth of information concerning critical exponents. Since our group at John Carroll University has been involved in acoustic and light scattering studies in the past few years, we decided to apply these techniques to the study of fluids near the critical point.

Studies of the propagation of sound in fluids have yielded interesting data on critical point behavior. A summary of experimental results obtained prior to 1965 is presented by Sette [20]. In studies performed recently in the Physics Department of John Carroll University we have been able to extend the range and precision of such methods. Our results are summarized in later sections of this report. In this section we will outline possible applications of acoustic techniques in studies of critical point phenomena.

5.1 Sound Velocity

For a single-component fluid in thermal equilibrium the sound velocity u in the critical region in general may depend on the frequency ν as well as the state variables P, T, and ρ. Thus we may write

$$u = u(\rho,T,\nu) \quad \text{or} \tag{24}$$

$$u = u(P,T,\nu) \tag{25}$$

Measurements of the velocity of sound yield directly the adiabatic compressibility κ_S, and this too may be expressed in the same manner:

$$\kappa_S(\rho,T,\nu) = \rho^{-1}u^{-2} \tag{26}$$

Here $\kappa_S(\rho,T,\nu)$ is equal to the thermodynamic or static compressibility only if the period $1/\nu$ of the acoustic waves is long in comparison to the relaxation time of any rate dependent processes affecting sound propagation in the fluid. Therefore, sound velocity measurements should be made at the lowest possible frequency to insure that the thermodynamic value of κ_S is obtained. On the other hand, measurements of u as a function of frequency may reveal the presence of rate dependent processes that are expected to be associated with critical point behavior.

If the sound velocity measurements are made at low enough frequencies to yield the static value of κ_S, the data can then be employed to determine the specific heat at constant volume C_V. The latter is given by expression

$$C_v(\rho,T) = T(\partial P/\partial T)^2_\rho[\kappa_s^{-1}V^{-1}+(\partial P/\partial V)_T]^{-1} \quad (27)$$

As the critical temperature is approached from above along the critical isochore, $(\partial P/\partial V)_T$ becomes small compared to $\kappa_s^{-1}V^{-1}$ and we may write

$$\lim\ (T\to T_c)C_v(\rho_c,T)\to T_c(\partial P/\partial T)^2_{\rho_c} V_c\kappa_s(\rho_c,T) \quad (28)$$

From this it can be seen that C_v and κ_s should diverge similarly along the critical isochore above T_c. Thus their behavior should be described by the same exponent α.

Sound velocity measurements, therefore, provide a method for determining the behavior of C_v which complements direct calorimetric methods. Since the latter yield values of C_v that effectively are averages over a small but finite temperature range, they have inherent errors that may become quite large in the vicinity of the critical point. As already pointed out, measurements of the sound velocity as a function of frequency also can yield information about rate dependent contributions to the adiabatic compressibility.

5.2 Sound Absorption

When an acoustic signal of frequency ν is propagated, energy is absorbed and the sound intensity I decreases with distance traveled. The energy absorption coefficient a for plane wave propagation is defined by the equation

$$I(x) = I_0 e^{-ax} \quad (29)$$

where I_0 is the initial intensity at x = 0. The absorption coefficient is a function of the thermodynamic equilibrium properties $\gamma^* = C_p/C_v$ and the sound velocity u, and also of the transport properties including the shear viscosity η, the bulk viscosity ζ and the thermal diffusivity λ'. It is usually written as [21]

$$a(\rho,T,\nu) = \frac{4\pi^2\nu^2}{u^3}\left\{\frac{\zeta + 4/3\eta}{\rho} + \lambda'(\gamma^* - 1)\right\} \quad (30)$$

This expression for a applies as long as the energy absorption per wavelength $a\Lambda$ is small. Thus, in the critical region where a becomes very large, care should be taken in applying Eq. (30) without modification.

As indicated in Eq. (30), a is a function of a number of quantities that are expected to depend strongly on the state parameters in the critical region as well as on frequency. Fortunately, all but the bulk viscosity ζ may be measured using other techniques. Therefore, acoustic absorption measurements provide the one feasible method for determining ζ. This quantity is of great interest because it is related to the structure of the fluid and dynamic

changes of structure. Sound absorption measurements should provide information about the structural relaxation processes that are believed to occur in the critical region and measurements of a versus frequency may yield data on the rate constants associated with such processes.

It is appropriate to point out here that the shear viscosity coefficient η may be measured using an acoustic technique [22]. This is based on the determination of the damping rate of a mechanical resonator, such as a tuning fork or a torsional resonator, submerged in the fluid. In the critical region such a method appears to be more appropriate for measuring the shear viscosity than any based on macroscopic flow of the fluid. In addition, it also provides a method for determining η as a function of frequency, at least over the range from approximately 1 kilohertz to 1 megahertz, and thus for determining the possible existence of shear relaxation effects in fluids in the vicinity of critical points. This appears to be a necessity if one hopes to determine the bulk viscosity ζ from sound absorption studies.

VI. LIGHT SCATTERING STUDIES OF CRITICAL PHENOMENA

Since the advent of the laser, light scattering has developed into one of the most widely used tools for studying the properties of materials. In fluids, quantities such as the thermal diffusivity λ', the ratio of specific heats γ^*, the sound velocity u, the iosthermal compressibility κ_T, and the sound attenuation coefficient a, among others may be determined from analyses of the intensity and the frequency spectrum of the scattered light. When a light beam is incident on a fluid sample, the light scattered at any angle Θ with respect to the incident beam consists, in general, of at least three Lorentzian lines: one at the frequency ν_0 of the incident light (the Rayleigh line), and two frequency shifted components at $\nu_0 + \nu_B$ and $\nu_0 - \nu_B$ (the Brillouin-Mandel'shtam lines).

Very briefly, when a single-component fluid is brought into the critical region, the Rayleigh line becomes very intense and narrow in width. The frequency shift ν_B of the Brillouin-Mandel'shtam lines decreases and they also become broader. Detailed discussions of the theory and application of light scattering techniques in studies of critical phenomena are given in References [23] and [24]. Here we would like only to summarize pertinent results and indicate how these techniques may be employed to determine the behavior of several properties of single-component fluids in the critical region.

6.1 Integrated Scattered Intensity and Critical Opalescence

A perfectly homogeneous medium would scatter light only into the same direction as that of the incident beam. In 1910, Einstein, following a suggestion by Smoluchowski, showed that in a real fluid there is scattering in all directions due to thermal fluctuations in density and temperature which lead to fluctuations in the dielectric constant ε. Let us represent the wave vector of the incident light beam of wavelength λ by $\vec{k}_0$, where $|\vec{k}_0| = 2\pi/\lambda$, and the wave vector of scattered beam by $\vec{k}'$. Then the scattering vector $\vec{K}$ is defined as

$$\vec{K} = \vec{k}' - \vec{k}_0 \tag{31}$$

This relationship between the three wave vectors and their relation to the scattering angle Θ is sketched in the following figure:

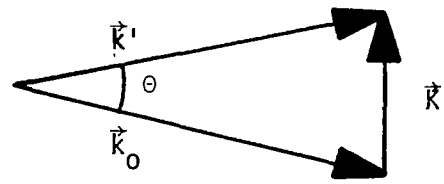

Note that for the case considered here, $|\vec{k}'| = |\vec{k}_0|$ to a very good approximation. Einstein showed that the intensity of the light scattered into a small solid angle about the direction $\vec{k}'$ satifies the proportionality

$$I(\vec{K}) \propto 1/\lambda^4 \langle |\Delta\varepsilon(\vec{K})|^2 \rangle \tag{32}$$

where $\Delta\varepsilon$ is the deviation of the local value of the dielectric constant from its equilibrium value. The bracketed factor is the average for the equilibrium ensemble. The symbolic form of the factor in brackets is meant to signify that the only fluctuations in the dielectric constant that contribute to the scattered intensity in the direction $\vec{K}'$ are those which have scattering vector $\vec{K}$.

The fluctuations in ε can be related to fluctuations in density and temperature; for a single-component fluid one may write

$$\langle |\Delta\varepsilon|^2 \rangle = \left(\frac{\partial\varepsilon}{\partial\rho}\right)_T^2 \langle |\Delta\rho|^2 \rangle + \left(\frac{\partial\varepsilon}{\partial T}\right)_\rho^2 \langle |\Delta T|^2 \rangle \tag{33}$$

Since $(\partial\varepsilon/\partial T)_\rho$ is usually small, Eq. (32) may be reexpressed in the form

$$I(\vec{K}) \propto \frac{1}{\lambda^4} \left(\frac{\partial\varepsilon}{\partial\rho}\right)_T^2 \langle |\Delta\rho(\vec{K})|^2 \rangle \tag{34}$$

Applying the thermodynamic theory of fluctuations, $\Delta\rho$ may be expressed in terms of the isothermal compressibility for the case for forward scattering, i.e. for $\vec{K} = 0$:

$$\langle |\Delta\rho(0)|^2 \rangle = \rho^2 k_B T \kappa_T \tag{35}$$

Here k_B is the Boltzmann constant. Substituting this into Eq. (34) one obtains the Einstein-Smoluchowski expression [25] for the forward scattered intensity:

$$I(0) \propto \frac{1}{\lambda^4} \left(\frac{\partial\varepsilon}{\partial\rho}\right)_T^2 \rho^2 T \kappa_T \tag{36}$$

From this it may be seen that a measurement of the total scattered intensity in the forward direction may yield information on the variation of κ_T in the critical region. Evidently, $I(0)$ should increase without limit in the critical region as κ_T diverges. This is just the phenomenon of critical opalescence, first observed by Avenarius in 1874 [26]. It should be pointed out that even far from the critical point, for $(T-T_c)/T_c \simeq 0.1$, the scattered intensity in the gaseous phase at critical density in the critical region far exceeds that of ordinary fluids away from the critical point.

The theory of scattering was extended to the case $\vec{K} \neq 0$ by Ornstein and Zernike in 1914 [27]. They realized that the probability of correlations between density fluctuations in adjacent volume elements becomes large in the critical region. When this is taken into account, the scattered intensity for small, but non-zero, $\vec{K}$ is given by

$$I(\vec{K}) \propto \frac{1}{\lambda^4} \left(\frac{\partial \varepsilon}{\partial \rho}\right)_T^2 \rho^2 \frac{T\kappa_T}{1 + (K\xi)^2} \tag{37}$$

where ξ is the long range correlation length (or Ornstein-Zernike correlation length). From the form of Eq. (37) one may deduce that in the critical region the scattered intensity diverges only in the forward direction, where $\vec{K} = 0$, since it may be shown that ξ^2 diverges in the same way as κ_T as T_c is approached.

6.2 The Spectrum of the Scattered Light

With the advent of the laser it has become possible to examine in great detail the spectrum of the scattered light. The high coherence and monochromaticity of the laser is required, expecially for studies of critical phenomena, since the Rayleigh line may be as narrow as several hundred hertz and the frequency shift ν_B of the Brillouin lines may be less than 500 MHz. With the use of single mode lasers source line widths of the order of several hertz are available and the optical resolution is therefore limited by the type of frequency analyzer employed to detect the scattered light.

The line widths and frequency shifts of the scattered light, even with a perfectly monochromatic incident beam, result from the fact that the fluctuations of density causing the scattering are not static in time. Examination of the scattered light spectrum, therefore, can yield directly information on the temporal behavior of the thermal fluctuations of the fluid. This is one reason why light scattering techniques provide such a useful tool for studying materials.

If the density is considered to be a function of entropy and pressure so that one may write

$$\Delta\rho = \left(\frac{\partial \rho}{\partial S}\right)_P \Delta S + \left(\frac{\partial \rho}{\partial P}\right)_S \Delta P \tag{38}$$

it is possible to deduce the following:

a) Those density fluctuations associated with entropy fluctuations satisfy a diffusion equation and decay exponentially in time. Therefore, they possess a frequency spectrum centered on zero and give rise to the Rayleigh line centered at the frequency of the incident light.

b) Those density fluctuations associated with pressure fluctuations may be looked on as satisfying a wave type equation and may oscillate in time as they decay. Therefore, they possess a frequency spectrum that may be peaked at other than zero frequency and so give rise to the Brillouin lines.

6.2.1 The Landau-Placzek Ratio

In terms of the above comments one may look on the Rayleigh line as due to scattering from entropy fluctuations at constant pressure that do not propagate. The Brillouin lines are due to scattering from thermal sound waves or phonons which propagate at the sound velocity u. An expression for the ratio of the integrated intensity of the Rayleigh line to that of the Brillouin lines may be calculated. It is given by

$$\frac{I_R}{2I_B} = \frac{\left(\frac{\partial \varepsilon}{\partial S}\right)_P^2 \langle |\Delta S|^2 \rangle}{\left(\frac{\partial \varepsilon}{\partial P}\right)_S^2 \langle |\Delta P|^2 \rangle} \tag{39}$$

This is known as the Landau-Placzek ratio [28]. With a few additional assumptions it may be transformed to the form

$$\frac{I_R}{2I_B} = \frac{C_p - C_v}{C_v} = \gamma^* - 1 \tag{40}$$

Since C_p is expected to diverge more rapidly than C_v near the critical point, this ratio may also diverge. Experimentally one does observe such an effect, i.e. there is a large increase in the intensity of the Rayleigh line compared with the Brillouin components for a fluid in the critical region.

6.2.2 The Thermal Diffusivity

One may obtain a measure of the mean lifetimes of entropy fluctuations τ_S by examining the width of the Rayleigh lines. Defining $\Delta\nu_R$ as the full width at the half intensity points one may show that τ_S is given by the relationship

$$1/\tau_S = 2\lambda' K^2 = 2K^2 T/(\rho C_p) = 2\pi\Delta\nu_R \tag{41}$$

Here $K = |\vec{K}|$ is the magnitude of the scattering vector and T is the thermal conductivity. Thus the lifetime is just the inverse of the angular frequency width. Rayleigh linewidth measurements therefore provide an elegant method for measuring the thermal conductivity. The first such measurements were made by Ford and Benedek [29]. The method allows measurements to be made very close to T_c where direct thermodynamic techniques break down. Since C_p goes to infinity and T, though large, varies much less rapidly, the linewidth $\Delta\nu_R$ approaches zero as T approaches T_c. It should be noted that because of the

very small thermal diffusivity near the critical point, it takes very long to achieve thermal equilibrium even though the thermal conductivity is large.

6.2.3 The Sound Velocity

Brillouin showed in 1914 [30] that one may determine the sound velocity u from the frequency shift ν_B of the doublet in the scattered light spectrum. One may show that at a scattering angle θ the doublet arises from scattering from thermal phonons of wave vector $\vec{K}$ and frequency ν_B and that the sound velocity $u(\nu_B)$ is given by

$$u(K) = 2\pi\nu_B/K \quad \text{or}$$
$$u(\nu_B) = C\nu_B[2n\nu_o\sin(\theta/2)]^{-1} \tag{42}$$

Here, C is the speed of light in vacuo, n is the index of refraction of the scattering medium at ν_o, the frequency of the incident light, and θ is the scattering angle. In ordinary liquids the portion of the thermal phonon spectrum over which measurements are practical, i.e. for scattering angles in the range 10° to 180°, lies in the range from about 1 to 6 GHz. Light scattering therefore provides a method for measuring the sound velocity at relatively high frequencies. It has proved to be of great use in determining the frequency dependence of the adiabatic compressibility in ordinary liquids and of fluids in the critical region. In the latter case, however, accurate measurements of the frequency shifts ν_B are made difficult because the Rayleigh line becomes so intense. In addition, the frequency shift ν_B becomes relatively small since the sound velocity decreases. When relaxation processes affect sound propagation, the scattered light spectrum may be modified and it may even contain additional frequency components [23, 31, 32, 33]. These may complicate the analysis and make the determination of the sound velocity difficult.

6.2.4 The Sound Absorption Coefficient

The line width $\Delta\nu_B$ of the Brillouin components in the scattered light spectrum is directly related to the lifetime of the thermal phonons, i.e. the pressure dependent density fluctuations. This lifetime, in turn, may be used to determine the effective sound absorption coefficient at frequency ν_B. Very simply, one may say that the greater the absorption, the shorter the lifetime and the broader the Brillouin lines in the spectrum, and vice versa. Quantitatively, one may write as a good approximation

$$\Delta\nu_B = \Gamma K^2/2\pi \tag{43}$$

Γ is the same factor as that occurring in acoustic measurements

$$\Gamma = \{\frac{\zeta + 4/3\ \eta}{\rho} + \lambda'(\gamma^* - 1)\} \tag{44}$$

Thus, in acoustic terms, we may write

$$a(\nu_B) = 2\pi\Delta\nu_B/u \tag{45}$$

It should be noted that care has to be taken in interpreting light scattering data in acoustic terms as was done in Eqs. (42) and (45), because in an acoustic experiment one makes measurements using a traveling or standing sound wave while in light scattering measurements one is obtaining information on the properties of thermal phonons [32, 34].

Consider Eq. (44) in the critical region. Since γ^* diverges, we may neglect 1 compared to γ^*. η is thought to show no anomaly and $\lambda'\gamma^*$ diverges relatively slowly [35]. Measured values of η and $\lambda'\gamma^*$ are too small to account for the measured values of $\Delta\nu_B$ or a in the critical region. Therefore, the bulk viscosity ζ must contribute substantially to $\Delta\nu_B$ and a. Thus, one can, in principle, determine the divergence of the bulk viscosity by studying the behavior of $\Delta\nu_B$ or the acoustic absorption. Ford, Langley and Puglielli [36] have made an attempt to deduce the behavior of ζ for SF_6 from their experimental Brillouin linewidth data. This is particularly interesting in the light of the prediction by Kadanoff and Swift [35] that for $2\pi\nu \leq \xi^{-2}\lambda'$ and for critical density at temperatures above T_c, $\zeta \sim \varepsilon^{-2}$, a very strong divergence. Equations (42) for the sound velocity and (45) for the Brillouin line width are applicable away from the critical region provided (a) the fluctuations may be described by the simple linearized hydrodynamic equations and (b) the width $\Delta\nu_B$ of the Brillouin lines is small in comparison to ν_B. We shall next list some corrections to these equations which may be applicable in the critical region.

6.2.5 Recent Modifications to Light Scattering Theory

As pointed out in section 6.1, recognition of the presence of long range correlations in the density fluctuations leads to modifications of the Einstein-Smoluchowski expression given in Eq. (36). Recently, Fixman has similarly modified the linearized hydrodynamic equations to include the effect of long range correlations that occur in the critical region [37] and Botch and Fixman [38] derived modified expressions for the Rayleigh and Brillouin line widths and the sound velocity in the critical region. These are given by

$$\Delta\nu_R' = \frac{\lambda' K^2}{\pi} \{\frac{1 + K^2\xi^2}{1 + K^2\xi^2/\gamma^*}\} ; \tag{46}$$

$$\Delta\nu_B' = \frac{K^2\Gamma'}{2\pi} \tag{47}$$

where $$\Gamma' = \{\frac{\zeta + 4/3\eta}{\rho} + \lambda' \left(\gamma^* - \frac{1 + K^2\xi^2}{1 + K^2\xi^2/\gamma^*}\right) \quad (48)$$

and $$u' = [1 + K^2\xi^2/\gamma^*]^{1/2} u \quad (49)$$

Since the long range correlation length ξ becomes large in the critical region these corrections to Eqs. (41), (42), and (43), respectively, should be considered in any detailed analysis of experimental data. Fortunately, one expects that the ratio of specific heats γ^* becomes large in the critical region so that these corrected expressions may be considerably simplified.

VII. DENSITY GRADIENTS

Due to the large isothermal compressibility of a fluid in the critical region, experimental studies of critical point behavior may be greatly complicated by the gravitational effects. Under ordinary laboratory conditions, i.e. in a normal gravity environment, a fluid sample is subjected to a pressure gradient due to its own weight. This gradient is given by

$$dP(z)/dz = -\rho(z)g \tag{50}$$

where z is measured vertically. This leads to a density gradient that may be written as

$$d\rho(z)/dz = -\rho^2(z)g\kappa_T(z) \tag{51}$$

for a fluid sample at constant temperature. Hence the density gradient will be large if κ_T is large. As the critical region is approached from above the critical temperature, κ_T diverges for $\rho = \rho_c$; thus the gradient $d\rho/dz$ will be greatest when $\rho = \rho_c$ and critical conditions can only exist in a thin horizontal segment of a fluid sample. This effect has been shown experimentally by Lorentzen [39] and Schmidt [40] who loaded chambers several centimeters in height with carbon dioxide gas so that the mean density was close to ρ_c. They observed optically the density gradient that developed in such chambers. Even for $T-T_c \simeq 0.03°C$ they detected density variations of more than 10% from the top to the bottom of the sample and noted that only a small fraction of the sample had density ρ_c.

The presence of density gradients may affect critical region measurements in a number of ways. The long range correlations believed to characterize critical behavior may not completely develop under normal g conditions. Kadanoff et.al. [5] have made simplified calculations that indicate one may neglect this direct gravitational effect in CO_2, for example, if $(T-T_c)/T_c >> 10^{-5}$, i.e. for $(T-T_c) >> 3$ millidegrees. Another effect of these density gradients in the critical region is that all experimental results, such as PVT and sound velocity data, obtained from measurements on finite height samples are averages over a range of densities rather than those for a unique density. Heller [41] has pointed out that much of the early PVT data obtained in the critical region may be in error because of the presence of such density gradients near T_c. Calculations of the effect of such averaging on the results of sound velocity measurements have been made by van Dael et. al. [42] and Ahlers [43]. Their results indicate that even the use of short cells ($\simeq$ 1cm in height) might not lead to improved precision because the density gradient is so sharply peaked at $\rho = \rho_c$.

Another possible effect is that the density gradient is itself a macroscopic form of ordering that may contribute to a measurable reduction in entropy and therefore directly affect specific heat measurements and also determinations of other thermodynamic variables.

Fortunately various types of optical measurements will not be affected directly by the presence of density gradients. In light scattering studies, for example, it is possible to probe very small regions of a sample. In addition, optical methods may even utilize the gradients to obtain useful information. For example, by employing Lorentzen's method [39] of detecting the density gradients by determining the index of refraction n as a function of sample height one may obtain PVT data. Similar experiments have been performed by Schmidt and Traube [40,44] with improved equipment. In applying this latter method one assumes that the Lorentz-Lorenz equation remains valid in the critical region:

$$\frac{n^2-1}{n^2+2} = \frac{4\pi\rho}{3}\Omega \tag{52}$$

where n is the refractive index and Ω is the molecular polarizability which is assumed to remain constant. No reliable experimental data contradicts these assumptions, while theoretical calculations for argon [45] indicate that any corrections are less than 1 part in 10^4 in the critical region.

In addition to gravity induced density gradients one must also consider those due to temperature gradients. The thermal expansion coefficient $\alpha_p = -\rho^{-1}(\partial\rho/\partial T)_p$ diverges in the critical region and temperature gradients therefore will have much the same effect on density as pressure gradients. For example, it may be shown that a temperature difference of 1 millidegree across a 2.5 cm high sample of CO_2 produces a density gradient of magnitude comparable to that produced by the gravitational pressure difference which is of the order of .001 atm near T_c and ρ_c. In addition to static inhomogeneities, temperature gradients also may induce dynamic processes within a sample leading to macroscopic flow and other disturbing effects.

VIII. EXPERIMENTAL ASPECTS OF THE PRESENT STUDY

8.1 Experimental Techniques Employed

In previous sections we have discussed in general terms pertinent aspects of thermodynamic behavior of fluids in the critical region and various properties that may be measured using acoustic and light scattering techniques. We turn now to the specific experimental techniques and procedures that have been developed for critical point studies by our group in the Physics Department of John Carroll University during the past several years under NASA Grant NGR-36-006-002.

A resonant cavity method has been developed for sound velocity measurements in the low kilohertz range. Promising results have already been obtained in carbon dioxide and sulfur hexafluoride in the critical region and the method currently is being improved to increase its precision and range of application. Basically we measure the velocity of sound by determining the resonant frequencies of fluid filled cylindrical cavities with plane ends. If the cavity has rigid walls, and is of length ℓ and radius a, the resonant frequencies are given by [46]

$$\nu_{q,r} = u/2 \left[(q/\ell)^2 + (r_{mn}/a)^2\right]^{1/2} \tag{53}$$

where q is any positive integer and the r_{mn} are the n roots (including r_{oo}) of the equation $d[J_m(\pi r)]/dr = 0$. $J_m(\pi r)$ are the Bessel functions of the first kind. The various values of q and r_{mn} define the successive resonant frequencies. They arise from the condition that the particle velocity is assumed to vanish at the plane ends and at the cylindrical wall of the cavity. The longitudinal modes, corresponding to plane waves propagating back and forth parallel to the axis of the cylinder, are characterized by $q \neq 0$ and $r_{mn} = r_{oo} = 0$. More complex modes are characterized by $r_{mn} \neq 0$. The first set of non-symmetric modes occur for $r_{mn} = r_{10} = 0.586$, while the first radial set corresponds to $r_{mn} = r_{01} = 1.292$. It proves to be most convenient in measuring u to determine the frequencies of the longitudinal modes since they are simply integral multiples of the fundamental mode $\nu_o = u/2\ell$ and are therefore easily identified.

We have also measured the velocity of sound in carbon dioxide and sulfur hexafluoride at 1 MHz using a modification of the acoustic interferometer technique [47, 48]. Here again one determines the longitudinal modes of a much shorter cylindrical acoustic cavity but instead of varying the frequency as in our kilohertz system we vary the path length by moving a piston reflector. The piston forms one plane end of the cavity while a quartz crystal or other type of piezoelectric plate forms the opposite end. We first employed this method because it also provides a mechanism for determining the acoustic absorption coefficient. Effectively, in this technique one measures the impedance of an acoustic transmission line (i.e. the fluid column) by measuring its loading effect on the piezoelectric plate that is used to excite the cavity. By determining the resistive loading of the fluid column as a function of column

length one may obtain the absorption coefficient. This method has the disadvantage that the piston reflector must be moved. In the critical region such motion can introduce disturbing effects. Our most recent results indicate that it may be possible to determine a by measuring the quality factor of the resonances in fixed path length cavities. We have already obtained promising results in the kilohertz region using this latter method and we plan to test it in the megahertz range.

We have also set up several systems for studying the spectrum of light scattered by simple fluids in the vicinity of the critical point. These have been used to obtain preliminary data on the velocity of sound at high frequencies in sulfur hexafluoride. As already mentioned in Section 6.2.3 this is accomplished by measuring the frequency shift ν_B of the Brillouin components of the scattered light spectrum. While setting up these light scattering systems we also became interested in examining with optical techniques the macroscopic behavior of fluids in the critical region. We have obtained preliminary data on the development of density gradients and other macroscopic processes occuring in sulfur hexafluoride in the critical region.

8.2 Experimental Procedures

8.2.1 Temperature Measurement Systems

We have set up several systems for the measurement of temperature to the accuracy and precision required for critical region studies of the type we are performing.

For accurate calibration and measurement of temperature we employ three separate platinum resistance thermometers. These have been calibrated by the National Bureau of Standards over the temperature range of interest. One is maintained as a standard, used solely to periodically check the other two which are used as working standards in individual test systems. Two precision Mueller resistance bridges are employed to measure the thermometer resistances. Periodically we check the precision of our temperature measuring technique using a commercial water triple point cell. We have concluded that the absolute accuracy of our resistance thermometer measurement procedures is ± 0.002°C in the range between 10 and 60°C. No attempt has been made during the present study to determine the absolute temperature to any higher accuracy.

For measurement of precise temperature changes during experimental runs we employ Hewlett-Packard quartz thermometers. These greatly simplify temperature measurements and also make possible short term temperature measurements precise to 0.0001°C. Since these latter thermometers reportedly are subject to long term drift as well as hysteresis when they are temperature cycled, we have employed them mainly to measure temperature differences and have used a resistance thermometer in the temperature control bath to periodically establish the absolute temperature. To check on long term drift and hysteresis we examined the accuracy of four different quartz probes as they were cycled from 20°C to 60°C to 20°C over a five day period. We found that they indicated a

maximum deviation of ± 0.008°C from the temperature as determined with a calibrated platinum resistance thermometer, while the root mean square deviations for three separate temperature cycles was less than ± 0.004°C. This accuracy has been maintained over a period of four months so that we have concluded that the quartz thermometers may be used for absolute temperature readings accurate to ± 0.005°C without the need for frequency calibration.

8.2.2 Temperature Control Systems

The acoustic cells are submerged in temperature controlled 15 gallon liquid baths to maintain their temperature constant to ± 0.001°C. Commercially available proportional control servo units are employed to control the bath temperature. The sensing element for these is a platinum resistance thermometer placed within the bath in the vicinity of the test cell. Variable speed stirrers are used to vigorously agitate the coolant. Two electrical heaters are used in each bath, a 1000 watt heater to rapidly increase the temperature and a much smaller one which is actuated by the proportional controller. A refrigerant may also be circulated through a coil placed in the bath for quick cooling. These temperature controllers permit the temperature to be adjusted to an accuracy of 0.002°C reproducibly and are capable of holding the temperature constant to ± 0.002°C for several days.

For the light scattering studies we employ a similar 20 gallon temperature control bath. From this bath the temperature controlled fluid is pumped through a small secondary bath containing the windowed optical cell. The bath containing the cell is mounted on an optical bench. Due to the fact that the heat loss in the connecting tubing depends on the ambient temperature, temperature control is not as good as with the single unit temperature baths described above.

8.2.3 Cell Filling Procedure and Pressure Measurement

The acoustic and light scattering cells are filled with the fluid under test using the system shown schematically in Fig. 3. After the cell parts have been carefully cleaned by washing in solvents and detergent solutions and rinsing in distilled water, the cell is assembled and placed in the temperature control bath and connected to the filling system with a quick-connect fitting. With valve V_1 to the fluid supply bottle and vent valve V_5 closed, and all other valves open, the system is evacuated using a cryogenic vacuum pump. The pressure is reduced to approximately 0.5 microns and held at that pressure for approximately 1 hour. Valve V_2 is closed and V_1 is opened to admit fluid into the system. The temperature of the control bath is brought to a value approximately 5 to 10 degrees above T_c where satisfactory PVT data is available for the fluid. Some fluid is transferred from the supply bottle until the pressure in the system is brought to approximately the desired value and then V_1 and V_3 are closed. The pressure lines from V_3 to the cell and pressure gauge are wrapped with electrical heating tapes. Varying the line temperature provides

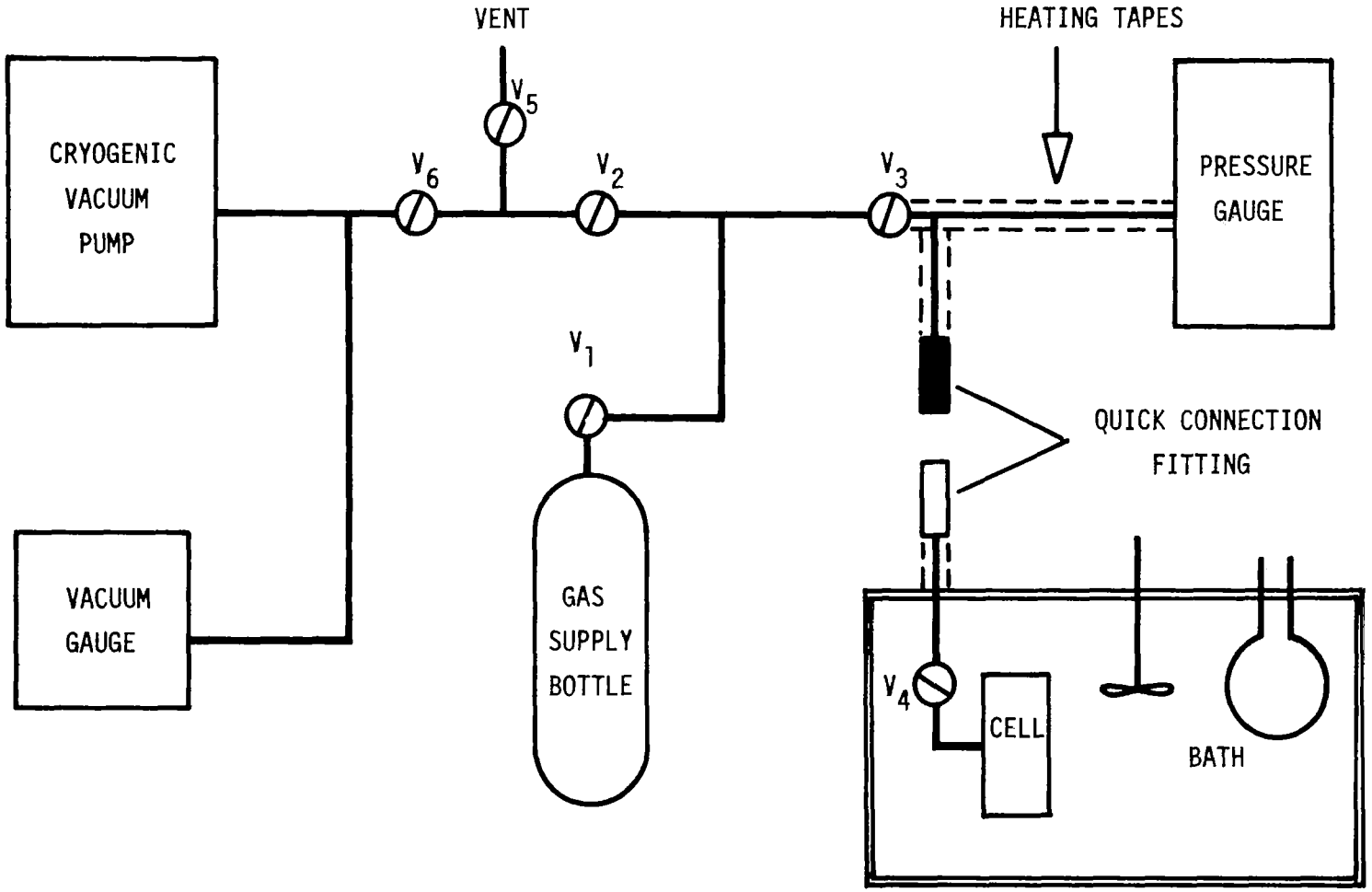

FIG. 3. FILLING STATION

a mechanism for finely adjusting the pressure in the test cell. When it is at the desired value, valve V_4 is slowly closed as the pressure is finely adjusted to the desired value. After V_4 is closed, the cell may be removed to another location if measurements are to be made at constant mean density as a function of temperature.

When measurements are made as a function of pressure, i.e. with valves V_4 open and V_3 closed, the heating tapes provide a convenient method of adjusting the pressure in the cell. It should be noted that the valves in the filling system are all-metal bellows type units to avoid contamination of the fluid samples.

The pressure gauge used in the present study is a Texas Instrument Co. unit having a stainless steel Bourdon tube for measurements to 100 atmospheres. This instrument may be used to make absolute pressure determinations accurate to ± 0.05 atm and relative measurements to ± 0.005 atm over a twelve hour period.

For CO_2, isotherm data [49] at 40.00°C were employed to fill the cells to the desired density. In this case, an error of ± 0.05 atm in the filling pressure at this temperature would lead to an uncertainty in the density of ± 0.0015 g/cm^3 or 0.3% near critical density. To fill the cells with SF_6 we employed 49.86°C isotherm data of Clegg et al [50]. They quote values of 0.73 to 0.75 g/cm^3 for the critical density. A recent calculation of physical properties and virial coefficients of SF_6 [51] gives a preferred value of 0.737 g/cm^3 for the critical density. While the filling procedure discussed above produces a small uncertainty in the filling density for CO_2, the uncertainty is relatively large for SF_6, mainly because the 49.86°C isotherm is too close to T_c and, hence, it is already quite flat. The next higher isotherm of Reference [50] is at 75°C, too high for our temperature bath. An error of ± 0.05 atm at 49.86°C leads to an uncertainty in the density of ± 0.015 g/cm^3 or 2% near critical density. This is to be compared to the 0.3% uncertainty for CO_2. After applying a correction for the pressure head due to the difference in height between the pressure gauge and the cell, we find ρ_c = (0.70 ± 0.02) g/cm^3 using the data for the 49.86°C isotherm of Reference [50].

8.2.4 System for Acoustic Measurements in the Low Kilohertz Range

The test cell employed for the low kilohertz acoustic measurements is sketched in Fig. 4. A cylindrical chamber 1.15 cm in diameter was bored in a 3.16 cm cross section brass hexagonal rod. The ends of the chamber were terminated with 1.25 cm diameter Bruel and Kjaer condensor microphones, one of which served as a source to excite the cavity and the other as a receiver to detect the amplitude of the acoustic pressure developed at resonance. Two such cells were used for the measurements reported here, one measuring 4.26 cm between the diaphragms of the condenser microphones, the other 3.78 cm. Care was taken to employ only metal and glass elements in that portion of the cell that came in contact with the fluid under test. The electrical feedthroughs from the pressurized portion of the cell to the 1 atm surroundings, for example, were metal in glass elements. Unfortunately, a small amount of organic sealant

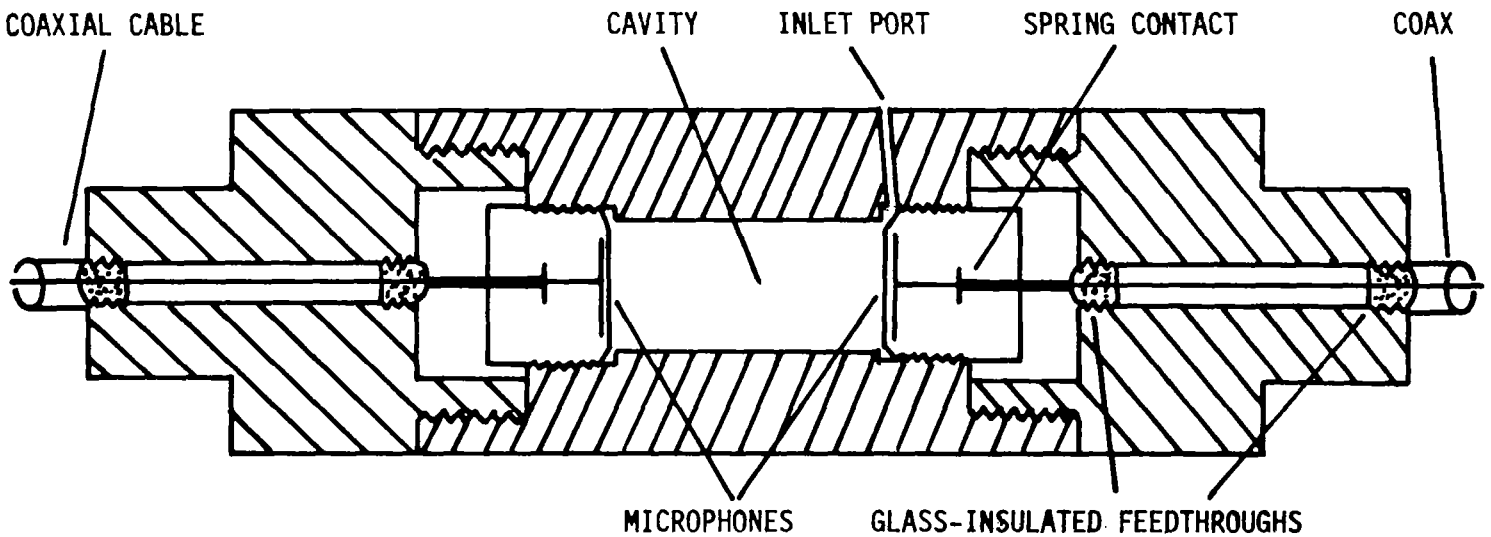

FIG. 4. ACOUSTIC RESONANCE CELL.

is used by the manufacturer of the microphones to secure a locking ring. We believe, however, that the effect of this sealant on the purity of the fluids and on their behavior in the critical region was negligible. The design of the cells is being changed, however, to eliminate this possible source of contamination in future measurements.

The test cell is submerged in the liquid bath in a location where substantial flow of liquid over all surfaces of the cell occurs. In portions of the measurement program provisions were made to orient the cell with its length either vertical or horizontal, though measurements were made usually in the vertical orientation. Either microphone could be employed as the sound source. The source was excited with the output signal from a stable audio oscillator and since no DC polarizing voltage was employed the acoustic frequency produced by the source was twice that of the applied voltage. Before amplification the signal from the receiving microphone was fed through a high pass filter to eliminate noise at frequencies below 400 Hz. Its amplitude was monitored with a precision voltmeter and its frequency displayed on a digital counter.

A given determination of the sound velocity was accomplished as follows. The contents of the cell were allowed to come to thermal equilibrium as indicated by stability of the resonant frequency of the cell and of the temperature. The latter was determined with the Hewlett-Packard quartz thermometer, the probe of which was in good thermal contact with the walls of the pressure cell. The audio oscillator was tuned to produce a maximum in the amplitude of the received signal at the lowest detected resonant mode of the cavity, corresponding to the fundamental longitudinal mode of frequency ν_0. The sound velocity under this condition is given by $u = 2\nu_0 \ell$ where ℓ is the effective length of the cavity. Care was taken to determine the fundamental mode at the filling temperature, i.e. well away from the critical region, where there was no ambiguity in determining the fundamental mode. Then as the temperature was decreased to approach T_c, the peak frequency corresponding to this fundamental mode was carefully followed since it decreased both in frequency and in amplitude as the critical region was approached. The temperature was changed in steps of decreasing ΔT and the equilibrium value of ν_0 was determined at each value of T to an accuracy of $\pm$ 1 Hz. Normally it was found that the attainment of a constant reading in ν_0 lagged behind the attainment of a constant reading of temperature by times of the order of 5 to 10 minutes. Data points taken at temperatures of less than one degree from T_c were usually recorded at 20 to 30 minute intervals. Using this procedure, it was found that the test cell could be left at the same temperature for periods of up to 24 hours and no measureable change in resonant frequency was observed.

It should be noted that the effective acoustic length of the resonant cavity appeared to be longer than the distance between the diaphragms of the condenser microphones. Such end effects are due to the motion of the diaphragms and we corrected for them by calibrating the acoustic length with a measurement of the velocity in air at 1 atm. This yielded a length ℓ approximately longer by 2 mm than the mechanically measured length.

One problem encountered with cells employing condenser microphones as source and receiver was that we sometimes noted random changes in the form of

the resonance peaks. Changing one or the other of the microphones usually had the effect of restoring the quality of the response to clean single peaks. This would seem to indicate deterioration of the microphones themselves. It was noted, however, that a pair of microphones having yielded poor response in one cell showed satisfactory response in the second.

8.2.5 System for Acoustic Measurements in the Megahertz Range

The acoustic interferometer employed for measurements at 1 MHz is sketched in Fig. 5. A cavity 2.2 cm in diameter was precision bored in a brass cylinder. For the measurements, the axis of this cylinder was vertical. A 1 MHz x-cut quartz disk was mounted in one end and the opposite end of the cavity was terminated with a moveable stainless steel piston. The piston was precision ground to fit in the cylinder with a tolerance of 0.0025 mm. The stem portion of a high pressure valve was employed as a leak-free mechanical feedthrough into the pressurized cell so that the piston could be moved to vary the length of the acoustic cavity. Though the motion of the valve stem introduces an undesired change of volume we felt that this source of error was relatively small. Other difficulties were encountered with this cell and only limited data on velocity and attenuation were obtained with it during our study. Experience gained using it has lead to the design of a fixed length cell which will be employed for future measurements in the megahertz range.

To make velocity and absorption measurements with the interferometer the quartz crystal was placed across the capacitance of a series resonant circuit. The output from a stabilized signal generator was used to excite the circuit. The signal generator and resonant circuit were tuned to the resonance frequency of the quartz transducer and a sensitive oscilloscope was employed to monitor the voltage across the transducer. In this arrangement the fluid filled cavity acts as an acoustic short circuited transmission line that goes in and out of resonance as the piston is moved. The velocity of sound may be determined by measuring the distance between locations of successive maxima or minima of voltage across the transducer, corresponding to a half wavelength change in the length of the cavity. The absorption coefficient is determined by measuring the rate of decay of the amplitude of the maxima and minima [52].

8.2.6 System for Light Scattering Measurements

Optics

The light scattering system is the most complex of the three experimental setups employed in this study. The complete system is shown schematically in Fig. 6. All of the optical elements are mounted on lathe bed type optical benches. A 0.1 milliwatt stabilized single frequency He-Ne laser is used as the light source. Its output beam passes through the aperture A and through two parallel glass plates mounted in precision gimbals. By moving these plates one is able to displace by a very small amount the laser beam perpendicular to the direction of propagation. This is useful during the aligning process. The beam passes through a small hole in the mirror M and enters the fluid cell through a flat circular area in the center of the conical window C. The beam is focused in the fluid under investigation. The unscattered light exits

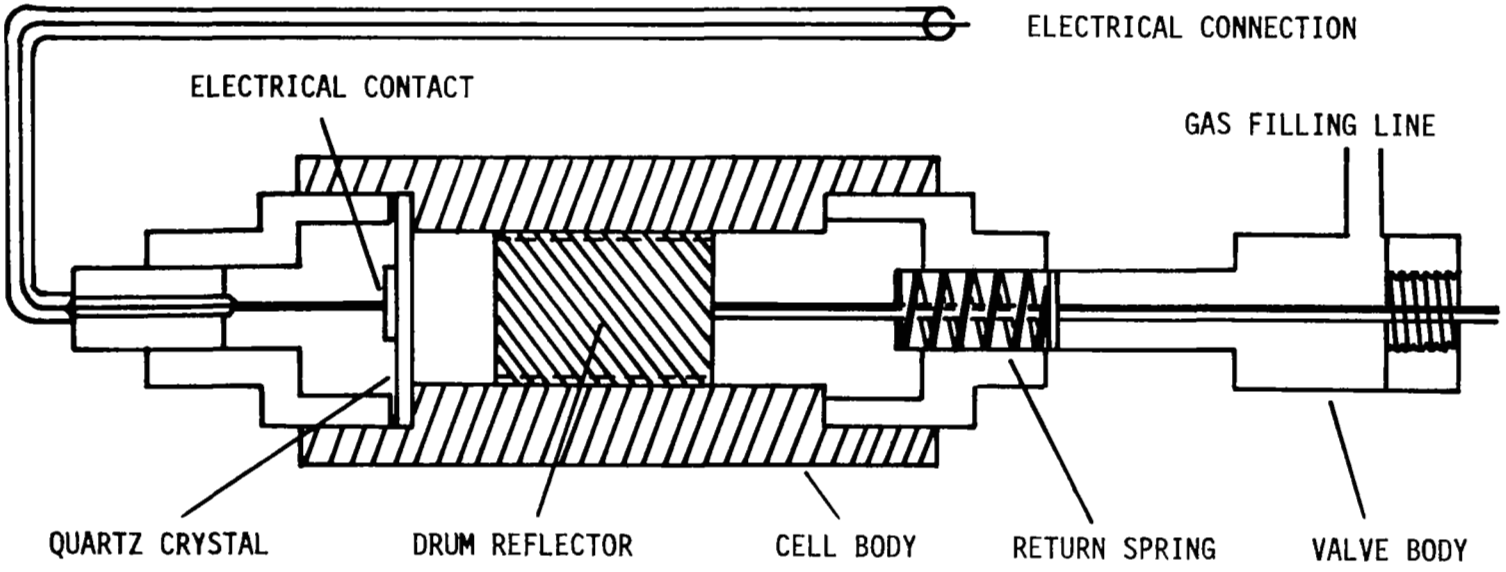

FIG. 5. ACOUSTIC INTERFEROMETER

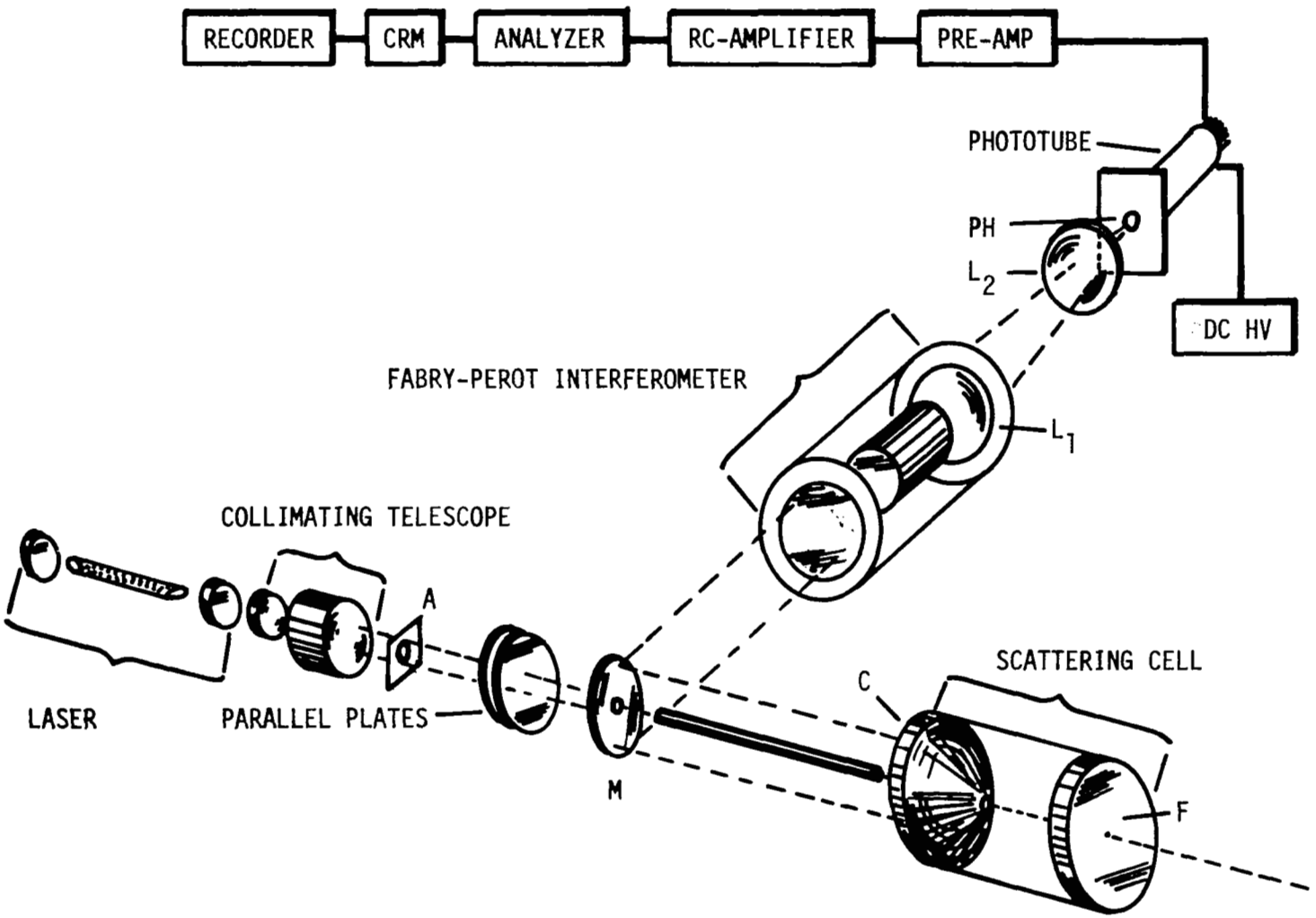

FIG. 6. EXPERIMENTAL LIGHT SCATTERING SETUP.

through the flat window F. Light scattered at an angle θ is collected by the conical lens, reflected from mirror M and it enters the Fabry-Perot interferometer. It is focused on the pinhole PH by means of the positive lens L_1 and the diverging lens L_2. The light which passes through the pinhole would form the center spot of the Fabry-Perot interference pattern and it goes on to the photosensitive cathode of the photomultiplier tube. This particular setup is described in greater detail by Fritsch [53].

Electronics

A small fraction (in this case approximately 8%) of the photons which strike the photo cathode eject electrons. Each of these are multiplied in the phototube to yield a burst of electrons at the anode. The bursts are preamplified, amplified further in an RC coupled system and then fed into the analyzer, which passes only those pulses exceeding a preset amplitude. The passed counts are recorded using a count rate meter and strip chart recorder.

This process is typical of nuclear counting techniques and the analyzer allows one to eliminate pulses due to noise and other extraneous processes. The single-photon counting system is described in more detail elsewhere [54-56]. This technique is superior to measuring directly the DC photocurrent in this application because the incident light level is extremely low and one is able to eliminate various noise components and also reduce the effect of leakage currents. Dark counting rates between 10 and 400 counts per second are typical.

Pressure Scanned Fabry-Perot System

The Fabry-Perot interferometer [57] used in this study is one we have constructed. It consists of two flat plates, 5 cm in diameter, dielectrically coated for 98% reflectivity at 6328 Å, separated by a low thermal expansion coefficient nickel-steel spacer. Three fine adjustment screws permit one to adjust the plates to 1/100th wavelength parallelism from outside of the pressurized housing of the interferometer. This latter arrangement is extremely convenient, since adjustments are frequently necessary. Spacers of length up to 14 cm, corresponding to an interorder spacing of 1 GHz have been employed with this unit.

The effective optical spacing of the plates may be varied linearly in time by changing the pressure and therefore the refractive index of nitrogen gas in the interferometer housing. This is accomplished by the use of a commercial linear sweep valve with added feedback and a large gas resevoir in parallel with the interferometer. In practice we have been able to obtain a linearly increasing pressure in the range desired from 1 to 1.8 atm at the required slow sweep rate of approximately 0.03 atm/hr.

The Light Scattering Cell

A cross section drawing of the high pressure light scattering cell is shown in Fig. 7. The flat and mushroom head conical windows are separated by a stainless steel spacer and the cell is sealed with O-rings. The design was

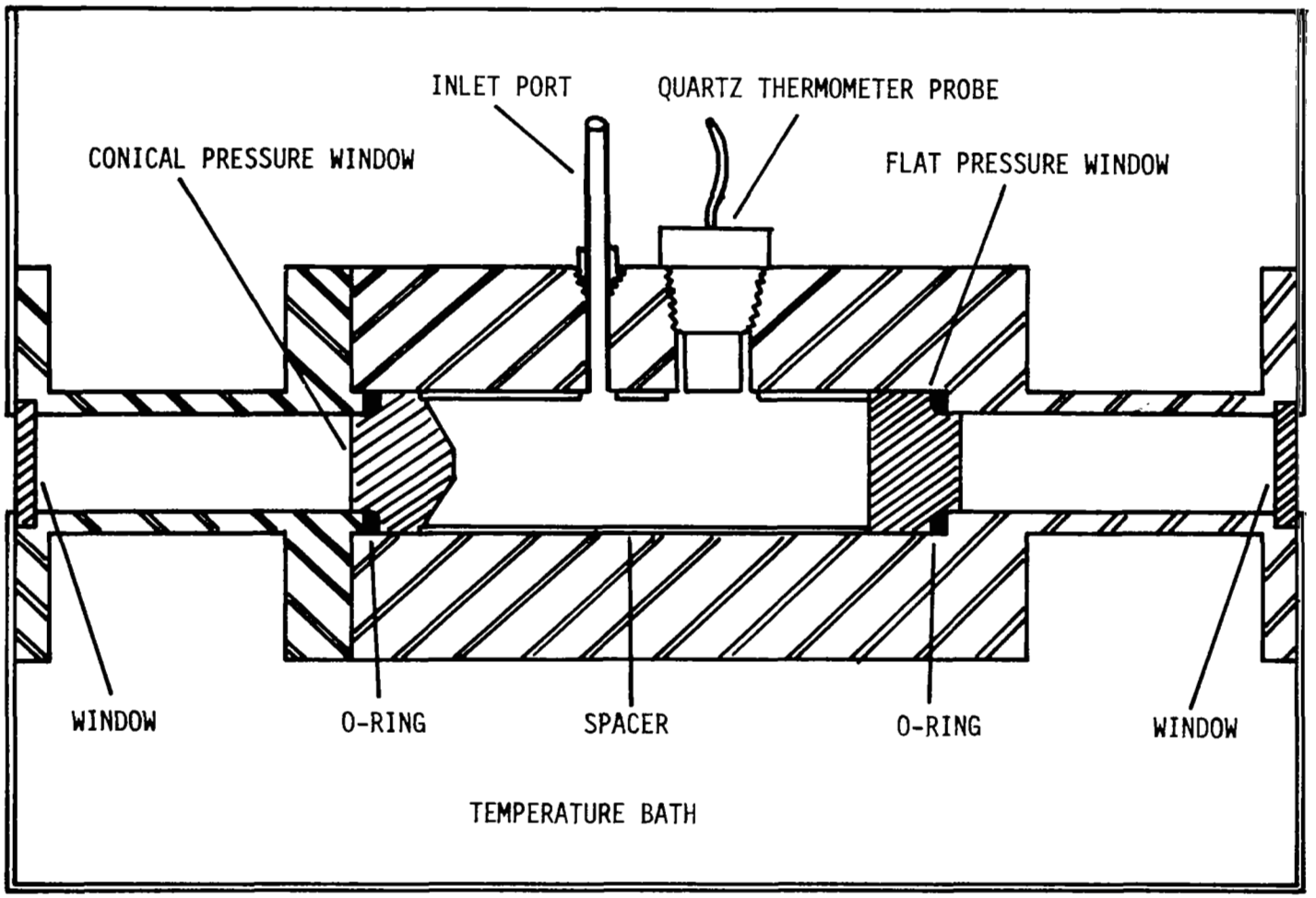

FIG. 7. LIGHT SCATTERING CELL.

suggested by Dr. Lastovka at M.I.T. The hole through the spacer is offset from its center line. Thus if the cell is loaded to critical density the meniscus will form either just above or just below the center flat portion of the conical window depending on the preset orientation of the spacer. In this way experiments can be done on either the liquid or the vapor phase at temperatures below T_c. The fluid cell is supported in the secondary temperature control bath by two sections of cylindrical tubing. Exit windows close the outside end of these tubes, which may be evacuated to reduce thermal leaks. A high pressure quartz thermometer probe is mounted in the cell so that the fluid temperature may be monitored directly.

IX. RESULTS

9.1 Acoustic Measurements in the Kilohertz Region

9.1.1 Carbon Dioxide

Our most extensive measurements were carried out in carbon dioxide in the kilohertz region. Data were taken both isochorically as a function of temperature and isothermally as a function of pressure in the one-phase region. Measurements in the two-phase region can also be carried out in the present cell. However, these yield an average of such quantities as the sound velocity and the sound absorption over the two phases. We did not carry out such measurements in the present study. The isochoric measurements are more easily interpreted theoretically than the isothermal measurements. To obtain accurate values for adiabatic compressibility κ_S and the specific heat C_V from these sound velocity measurements in the critical region we took the following precautions: (1) Measurements were made over a reasonably large range of $T-T_c$. (2) The test cell was made as short as possible to reduce the effect of gravitationally induced density gradients. (3) Low frequencies were employed to avoid velocity dispersion due to relaxation effects. (4) Measurements were made at constant density (isochorically) to facilitate a slow and reproducible approach to the critical point (or the coexistence curve). In the resonance technique used here conditions (2) and (3) are, in conflict, i.e. the desired low frequencies dictate the minimum height of the required cavity since it must be at least a half wavelength long. In the region of critical density the resonance frequency of this cell was 2400 Hz at $T-T_c$ = 10°C and decreased to a minimum of about 1200 Hz at the critical temperature. Such frequencies are well below the vibrational relaxation frequencies of CO_2 [58, 59]. Whether or not the velocities measured at these low frequencies are affected by other relaxation effects remains an open question.

When the critical point is approached along an isotherm, one tries to change the density by small amounts by varying the pressure. This is very difficult because of the extremely large isothermal compressibility of a fluid near its critical point. The advantage of approaching the critical point isochorically is that one may work with a closed cell which is not disturbed mechanically as the temperature is lowered by incremental cooling. For isochoric runs the cell was filled according to PVT data available for CO_2 at 40°C [49]. After filling to the desired density the cell was sealed and sound-velocity measurements were taken as the cell temperature was decreased in small increments. The sound velocity decreased to a minimum value and then sharply increased as condensation occurred. With average filling densities between 0.45 and 0.48 g/cm^3, minima in velocity ranging between 107 and 114 m/sec have been observed at temperatures between 31.04 and 31.12°C. These results are shown in Table III. For comparison, we have listed in Table IV the critical parameters for CO_2 reported by earlier investigators. The actual velocity versus temperature behavior for a density of 0.467 g/cm^3 is shown in Fig. 8. Using this and similar velocity data we have plotted in Fig. 9a the temperature dependence of κ_S calculated from the measured sound velocity data at densities

TABLE III Measured Velocity Minima in CO_2

Average Density (g/cm^3)	Velocity minimum (m/sec)	Temperature (°C)
0.45[a]	109	31.04
0.467	110	31.11
0.469	111	31.06
0.469	112	31.08
0.47[a]	107	31.11
0.47[a]	114	31.09
0.470	110	31.08
0.472	114	31.04
0.482	108	31.12

[a] These results were obtained with commercial grade CO_2; the other runs were obtained with research grade CO_2.

TABLE IV Critical Parameters for CO_2

Reference	ρ_c (g/cm^3)	T_c (°C)	P_c (atm)
Michels, Blaisse, Michels [60]	0.467	31.04	72.85
Lorentzen [39]	-----	31.04	-----
Wentorf [61]	0.477	31.05	72.84-72.87
Swinney [62]	-----	31.08	-----

of 0.467 and 0.469 g/cm^3, i.e. for two separate fillings at essentially critical density, and for a third filling at 0.482 g/cm^3. In each of the three cases, for the purpose of these plots, T_c was taken to be the temperature at which the minimum velocity was observed. The graph in Fig. 9a may be interpreted as indicating the existence of a logarithmic singularity in κ_S as the critical point is approached along the critical isochore. This logarithmic behavior seems to extend from $T-T_c \approx 20°C$ to $T-T_c \approx 0.02°C$. Logarithmic singularities

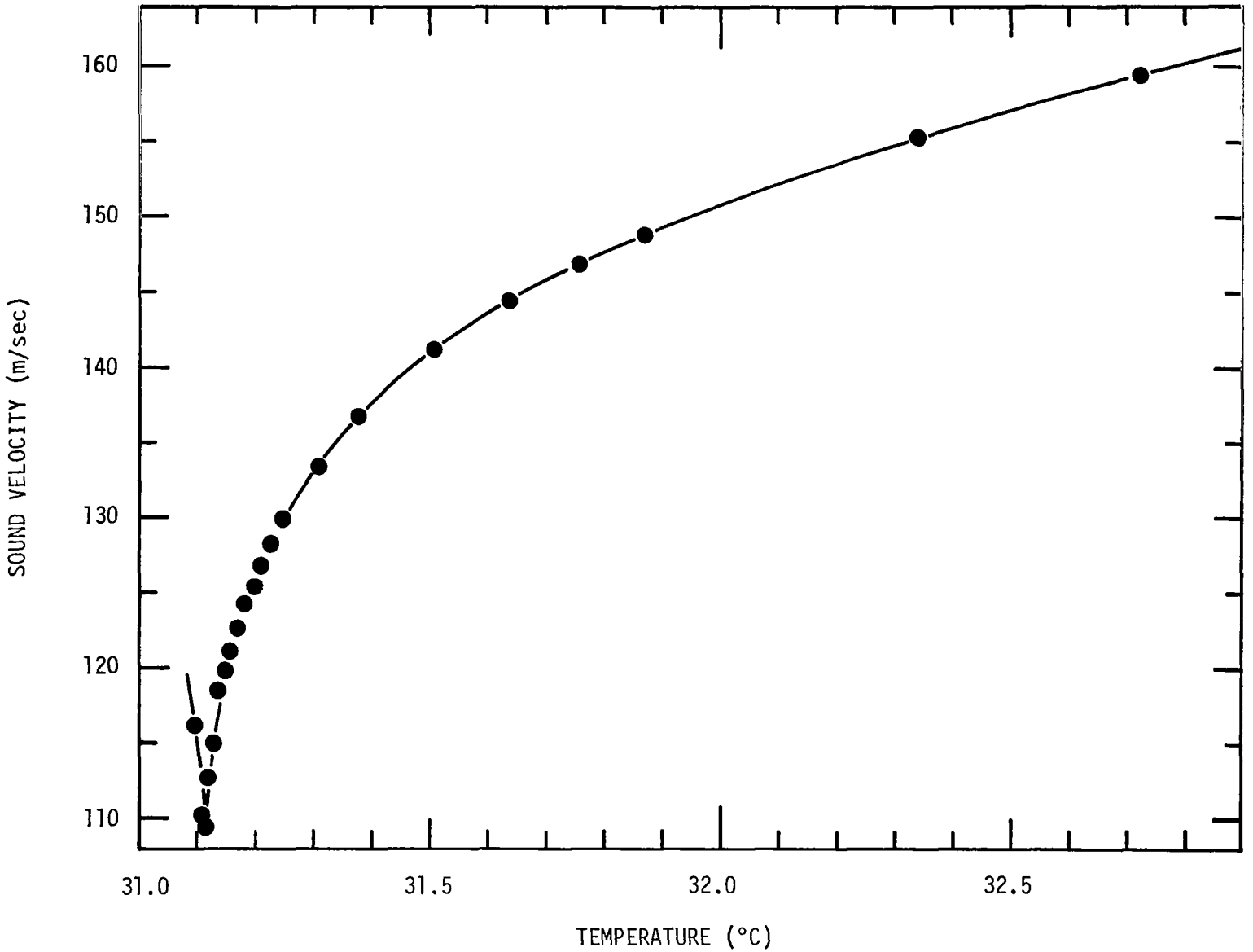

FIG. 8. SOUND VELOCITY AS A FUNCTION OF TEMPERATURE IN CO_2 AT CRITICAL DENSITY.

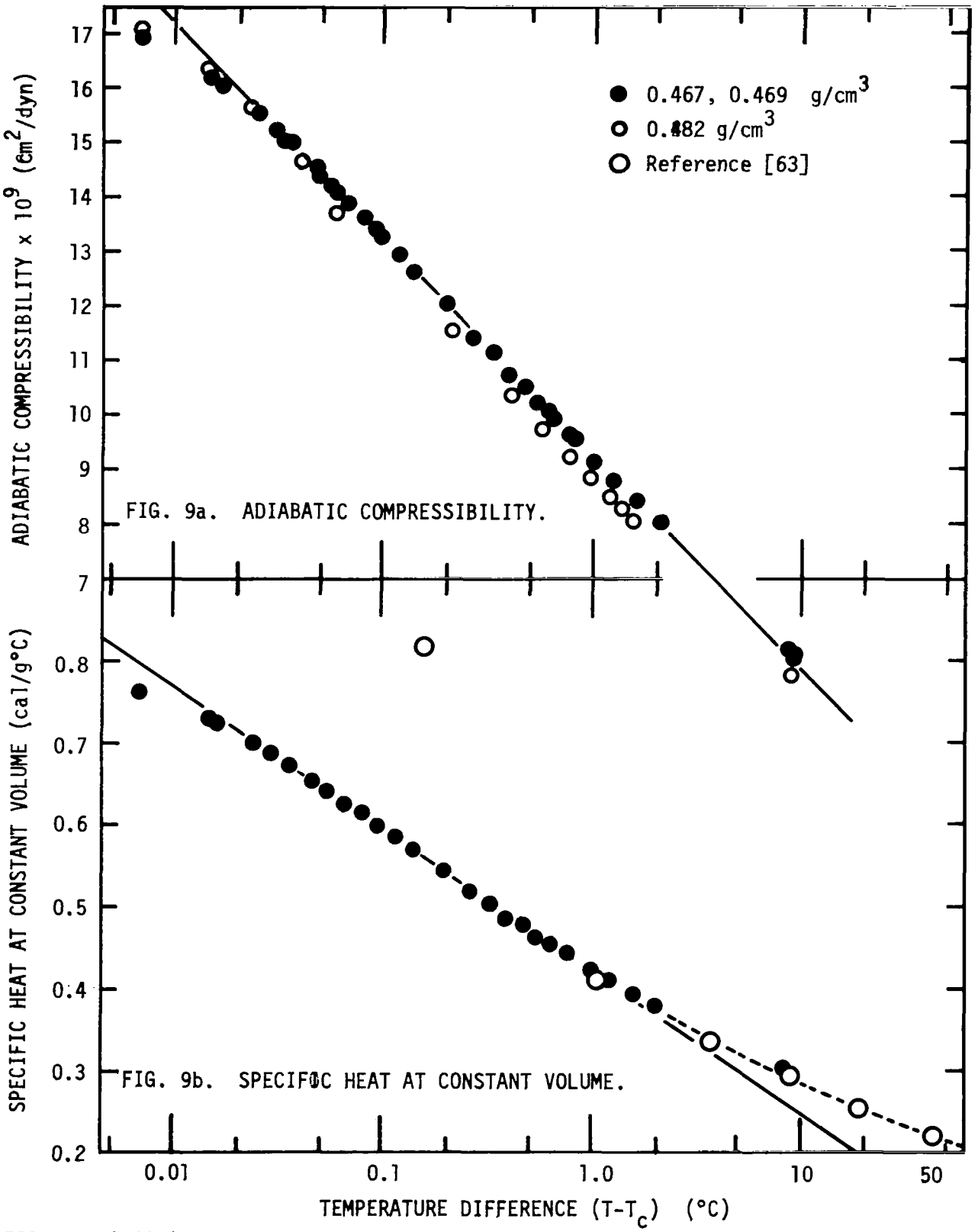

FIG. 9. ADIABATIC COMPRESSIBILITY AND SPECIFIC HEAT AS A FUNCTION OF $T-T_c$ IN CO_2.

in κ_S have been reported by Williamson and Chase [64] in He and by van Dael et al [42] in Ar. Previous sound velocity measurements in CO_2 [65-68] did not allow such conclusions concerning the critical exponents of κ_S. The behavior for a density of 0.482 g/cm^3 seems to be logarithmic over a much smaller temperature range.

The solid line in Fig. 9a represents a least squares fit to the experimental compressibility at critical density between $T-T_c$ = 20°C and $T-T_c$ = 0.02°C. The equation of this line is

$$\kappa_S = -0.55 - 1.72 \ln [(T-T_c)/T_c] \qquad (54)$$

where T_c = 304.20 K (the generally accepted value) and κ_S is in units of 10^{-9} cm^2/dyn. In Fig. 9b are presented the values of C_V calculated from Eq. (27) using our measured velocities on the critical isochore and the data for $(\partial P/\partial T)_V$ and $(\partial P/\partial V)_T$ from Reference [49]. As indicated, these calculated values of C_V are in excellent agreement with the experimental measurements of Michels and Strijland [63]. Their anomalously high value of C_V measured at $T-T_c$ = 0.16°C is probably due to the relatively large temperature increments they employed for their calorimetric measurements. The graph indicates logarithmic behavior of C_V for 0.02°C<$T-T_c$<1°C. The solid line in Fig. 9b represents the least squares fit to the calculated C_V data in the above temperature range:

$$C_V = -0.005 - 0.075 \ln [(T-T_c)/T_c] \qquad (55)$$

with C_V in units of cal/g°C. Similar approximate logarithmic singularities in C_V at the critical points of Ar, O_2, Xe, and He observed in calorimetric measurements have been reported by Bagatskii, Voronel', and Gusak [69], Voronel' et al [9, 10], Edwards, Lipa and Buckingham [12], and Moldover and Little [13]. The behavior for 1°C<$T-T_c$<50°C observed here is of the form $(T-T_c)^{-0.16}$.

The graphs in Fig. 9 indicate that the experimental points begin to deviate from logarithmic behavior for $T-T_c$ less than 0.02°C. In this region, the measured velocities are higher than one would expect from a continuing logarithmic behavior. This latter effect may be attributed to the presence of gravitationally induced density gradients. Since our technique yields the acoustic travel time through the cell, each of the velocity minima listed in Table III prepresents an average value of the velocity which because of the existence of density gradients, is necessarily higher than the true velocity $u = u(\rho_c)$ for small values of $T-T_c$. One must go on to ask whether the effect of the density gradient on the measured velocities becomes important at $T-T_c$ greater than 0.02°C. More extensive data and calculations are required before a precise answer can be given. However, during our experiments we were able to turn the cell from the vertical to the horizontal position. This was done during a number of runs. Sometimes the whole run was carried out with the cell in the horizontal position. At other times, the cell was repeatedly turned between the horizontal and vertical position at each temperature. The velocities measured in every case were very close to those determined in runs in which the cell was maintained in the vertical position throughout the run. The height with the cell horizontal would correspond to 1.2 cm. However, these

results do not indicate that the density gradient may be neglected. As was pointed out before, the effect of the density gradients can only be eliminated if one goes to an extremely short cell. Furthermore, an effective averaging process also must have occurred for the horizontal orientation so that additional measurements made with much shorter cells are called for.

Even though isothermal measurements as a function of pressure are not as easily interpreted theoretically as isochoric measurements, we also made measurements of the sound velocity as a function of pressure to obtain information on the pressure and density dependence of the thermodynamic derivatives. As it turned out this data was quite helpful in our isochoric work and was more precise than we had expected. Therefore, this data is presented here along with conclusions that may be drawn from it on the density dependence of κ_S and C_V. In Fig. 10 we have summarized the data of the velocity of sound in CO_2 as a function of pressure at five different temperatures. The temperatures chosen are those for which PVT data is available [49]. In this way our results may be compared with available specific heat measurements, for example. It can be seen that the velocity versus pressure curves become extremely sharp near the critical point. This is precisely the reason why we made more extensive isochoric measurements than isothermal measurements. For clarification this same data is replotted in Figs. 11 through 14 for each of the temperatures at which pressure runs were taken.

Some remarks on these data are in order. It may be seen from Fig. 14 that in the vicinity of the minimum the velocity varies between 180 m/sec and 120 m/sec for a pressure change of 1 atmosphere. We were able to detect pressure changes of ±0.005 atm with the Bourdon tube gauge. Since over long periods there may be some drift in the gauge readings and also hysteresis when the gauge is cycled, the absolute pressure cannot be known to better than ±0.05 atm. The error may be slightly larger, since it is difficult to correct for the effect of the pressure head due to the height separation of the cell and the pressure gauge. In these isothermal runs we concluded that the coexistence curve was encountered on the 31.10°C isotherm, but not on the 31.20°C isotherm. Therefore, the effective critical temperature was somewhere between those two temperatures, in basic agreement with the data presented in Table III. This would put the critical pressure somewhere between 72.93 atm and 73.12 atm. The critical pressures observed by earlier investigators by direct visual observation are 72.85 atm [60] and between 72.84 to 72.87 atm [61]. The discrepancy between our value of P_c and these latter data makes it difficult to use the PVT data of Reference [49] to make calculations involving thermodynamic derivatives in the critical region. However, we did carry out some calculations for the 40.00°C and the 34.80°C isotherms and also for the 32.1°C isotherm, though in the latter case our results at best are only qualitative. First we replotted the data as a function of density using the above mentioned PVT data. This is shown in Fig. 15. It can be seen that the minima of the velocity versus density curves approach the critical density ρ_c close to T_c, but these minima occur at densities below ρ_c away from the critical point. Obviously it would be desirable to have obtained this data by measuring the density directly and we hope to be able to do such measurements in the future.

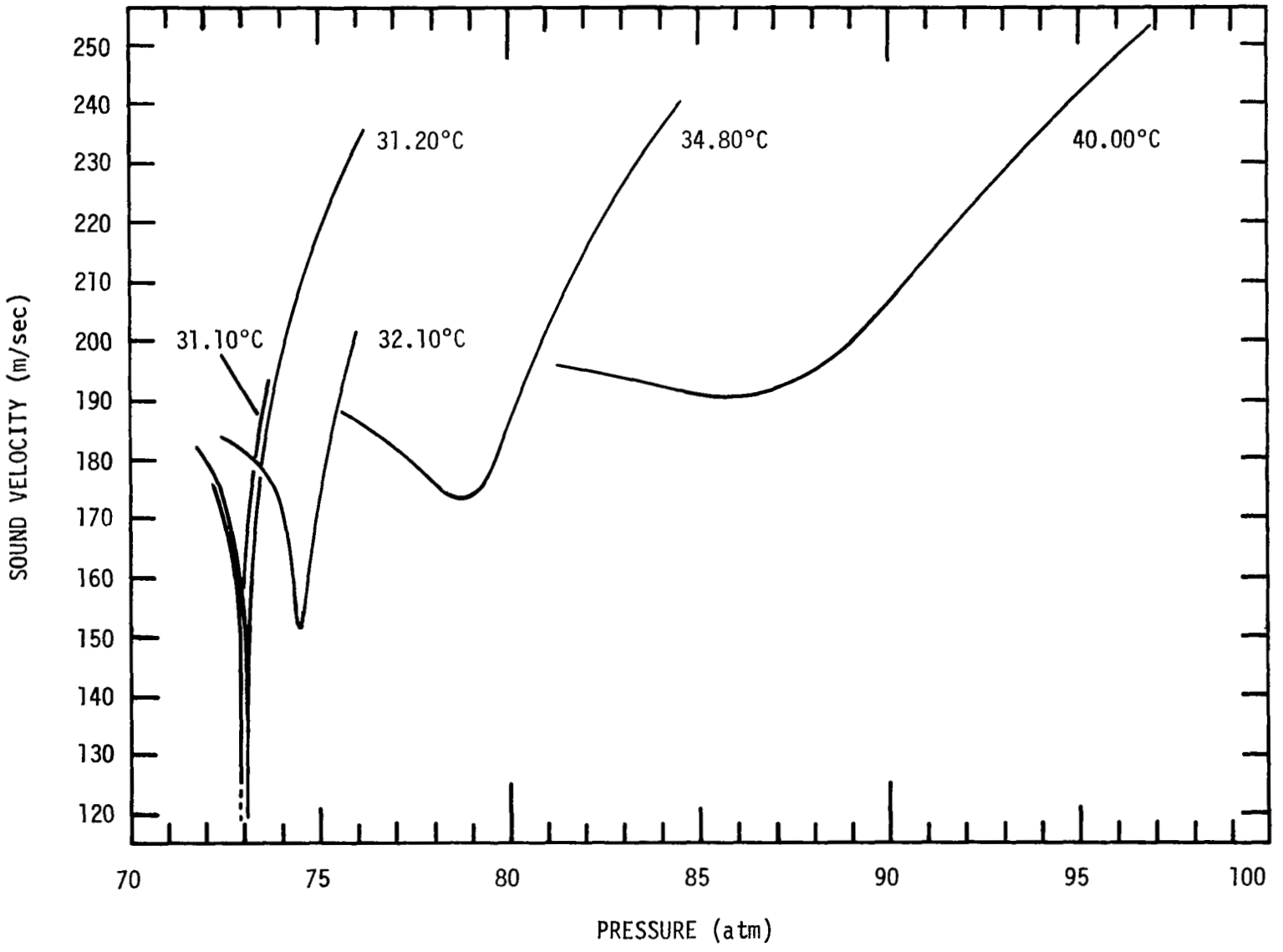

FIG. 10. SOUND VELOCITY AS A FUNCTION OF PRESSURE IN CO_2.

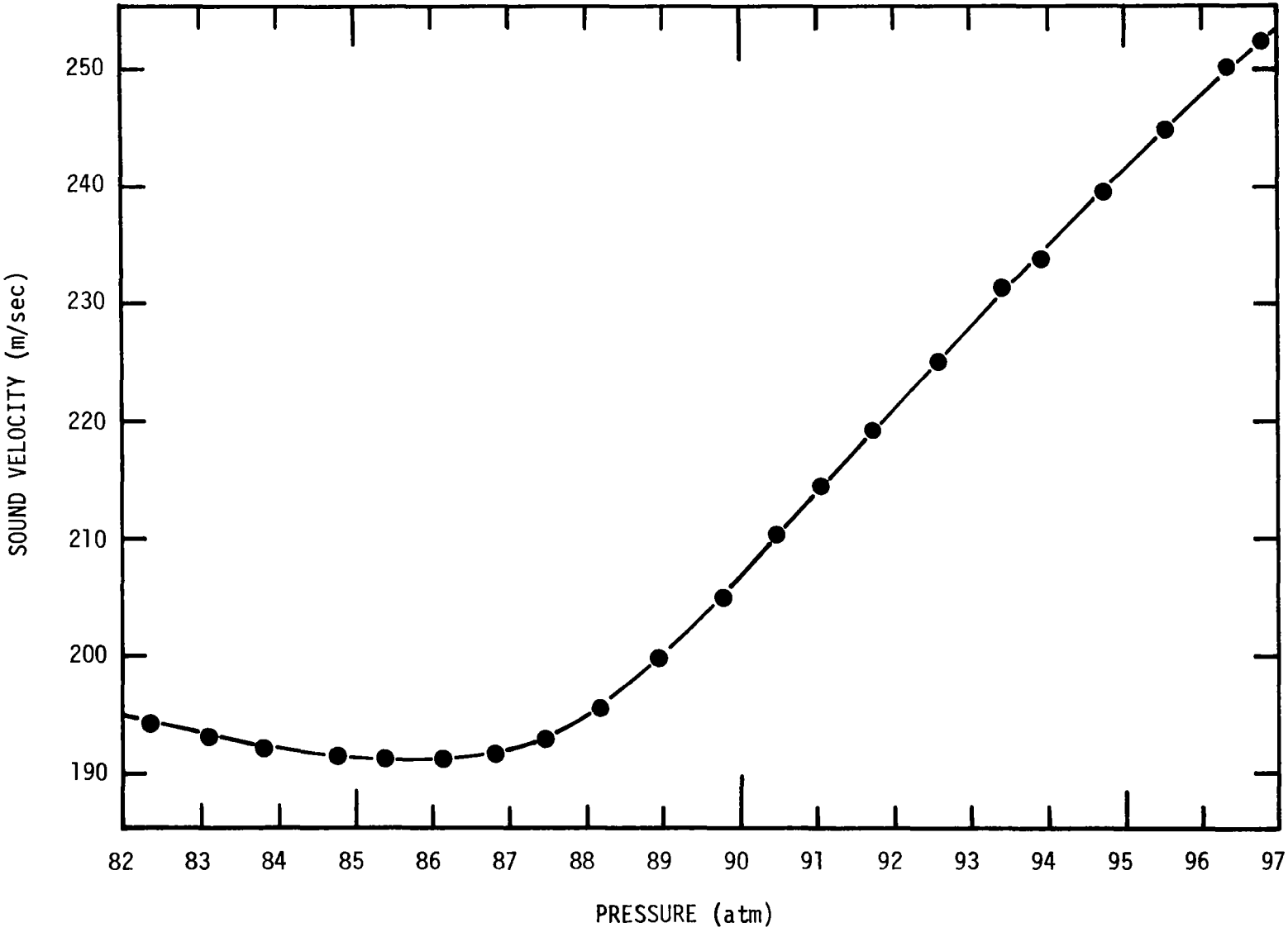

FIG.11. SOUND VELOCITY AS A FUNCTION OF PRESSURE IN CO_2 AT 40.00°C.

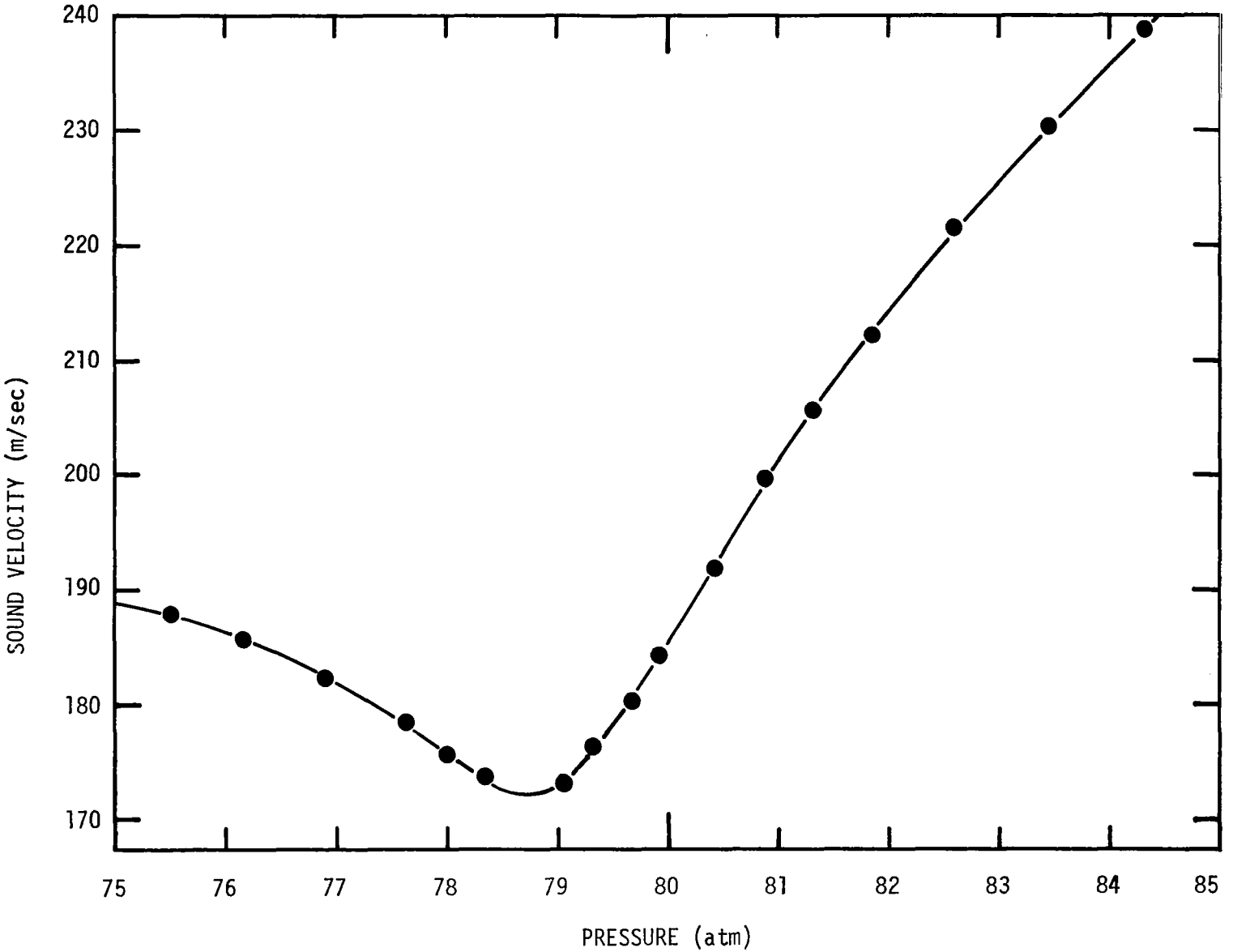

FIG. 12. SOUND VELOCITY AS A FUNCTION OF PRESSURE IN CO_2 AT 34.80°C.

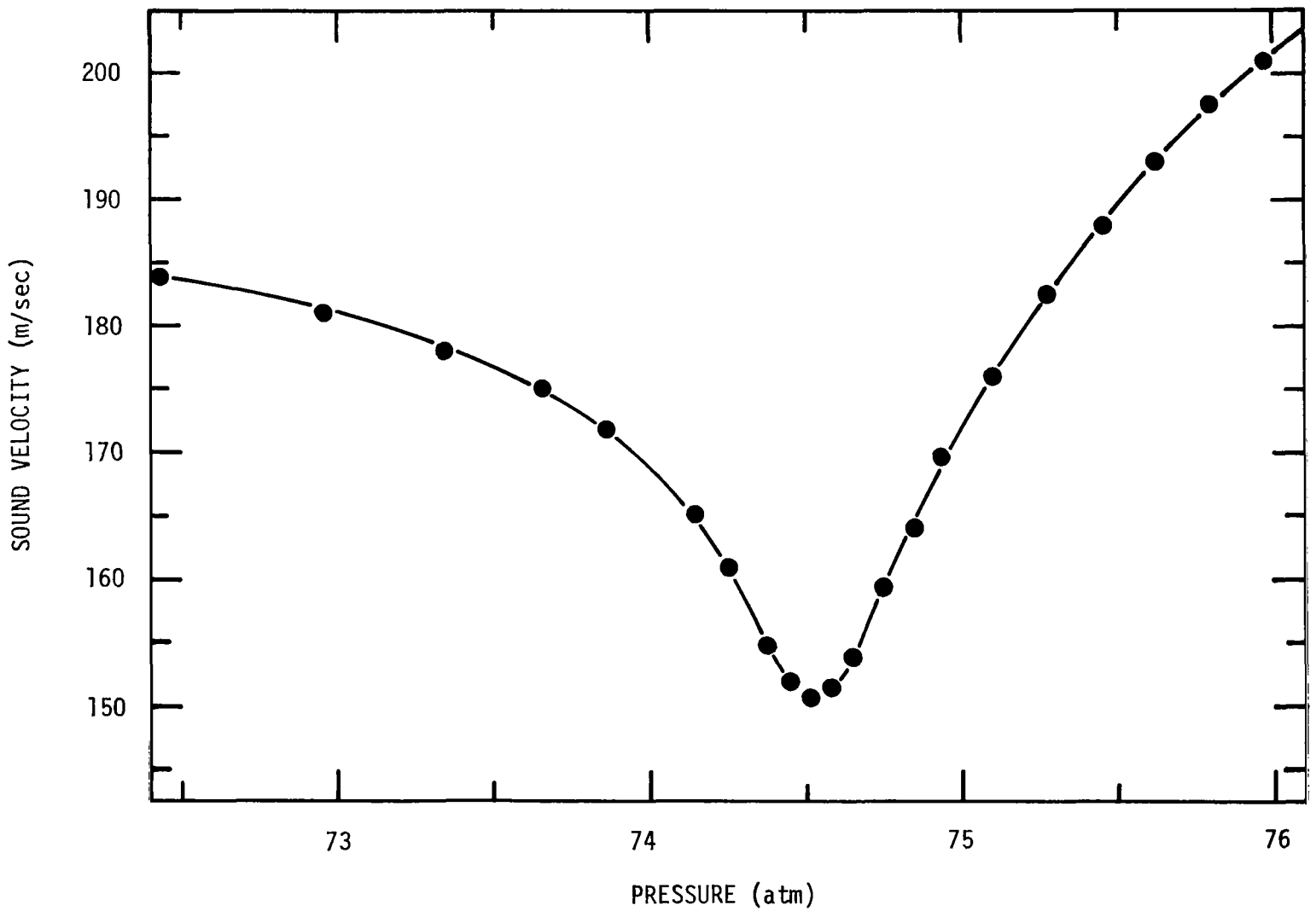

FIG. 13. SOUND VELOCITY AS A FUNCTION OF PRESSURE IN CO_2 AT 32.10°C.

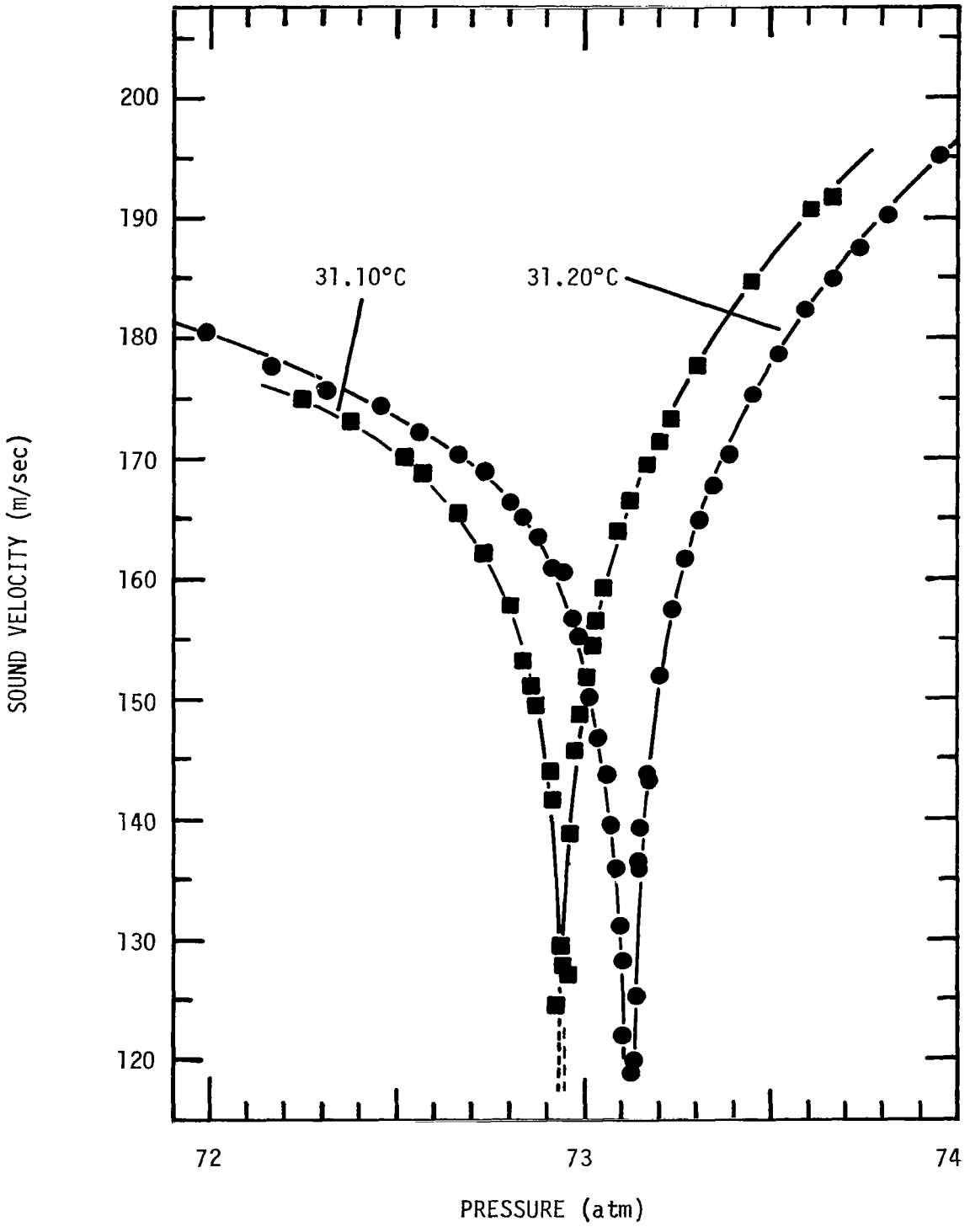

FIG. 14. SOUND VELOCITY AS A FUNCTION OF PRESSURE IN CO_2 AT 31.10°C AND 31.20°C.

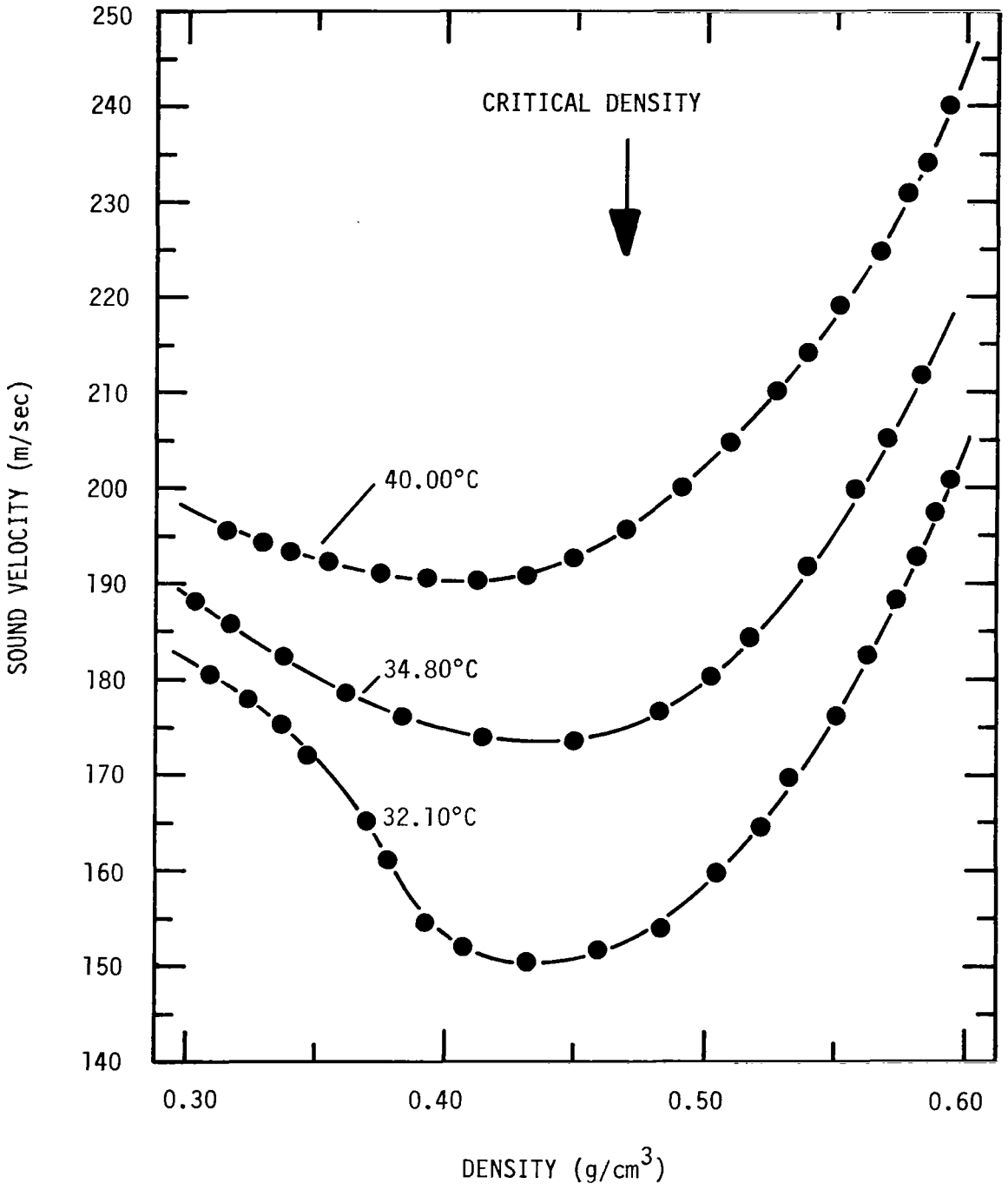

FIG. 15.. SOUND VELOCITY AS A FUNCTION OF DENSITY IN CO_2.

The adiabatic compressibility κ_S and the specific heat C_v are plotted in Figs. 16a and b, respectively, as functions of density at 40.0°C, 34.8°C, and 32.1°C. It may be seen that away from the critical region the adiabatic compressibility rises slowly as the density decreases. Near the critical point, a peak appears near or below critical density. This same behavior is exhibited by the isothermal compressibility [24]. The specific heat at constant volume is essentially independent of density, except that near the critical point a peak in C_v occurs. For comparison, the experimental data on C_v of Michels and Strijland [49, 63] has been included. The agreement between our calculated values and their calorimetric data is better than ±10% for the 40.00°C and 34.80°C isotherms. At 32.10°C the agreement is poorer. This is partially due to the difficulty of taking calorimetric specific heat data near the critical point. However, the shift between the peak in their experimental data and our calculated values may be due to the difficulties we noted above in interpreting our isothermal velocity data.

9.1.2 Sulfur Hexafluoride

Low frequency sound velocity measurements are being made in SF_6 using the resonant cavity technique. We began these using the condenser microphones, as in our CO_2 studies, but recently we have constructed new cells employing ceramic piezoelectric plates as sound transducers. Our preliminary results have been promising; in this way we have been able to eliminate the possibility of contaminating the fluid samples since only metal and ceramic elements contact the fluid once the cells are filled. The new cavity lengths are also shorter. We have taken extensive data with a cell 2.5 cm long and have begun to experiment with cells as short as 0.1 cm.

Data analysis for SF_6 is complicated by the fact that only limited PVT measurements in the critical region have been reported [50]. This has lead to some inconsistencies in interpreting our results. We consider here only data obtained for a single filling density. Using the filling procedure outlined previously, we loaded the test cell at 49.86°C, i.e. approximately 4°C above T_c, to a density which we calculated to be (0.69 ± 0.02) g/cm^3. This should be compared to our value of (0.70 ± 0.02) g/cm^3 for the critical density. This filling yielded the lowest velocity value we have measured for SF_6. This was 54 m/sec at 45.625°C, as indicated in Fig. 17, where we have plotted the measured sound velocity versus temperature. Table V presents the critical parameters of SF_6 as reported by earlier investigators. We have obtained a temperature of meniscus appearance in a slow unstirred cooling run of 45.57°C. The minimum in the sound velocity at approximately critical density appeared at 45.63°C.

The velocity measurements presented in Fig. 17 were obtained at frequencies ranging from 3 to 2 kHz, and we made them using the second harmonic of the fundamental longitudinal mode of a 2.5 cm cavity. This turned out to have the sharpest response at low frequencies. In addition we have taken measurements of velocity versus temperature using higher harmonics, e.g. the 20th to the 30th in the frequency range 30 to 40 kHz. From our preliminary

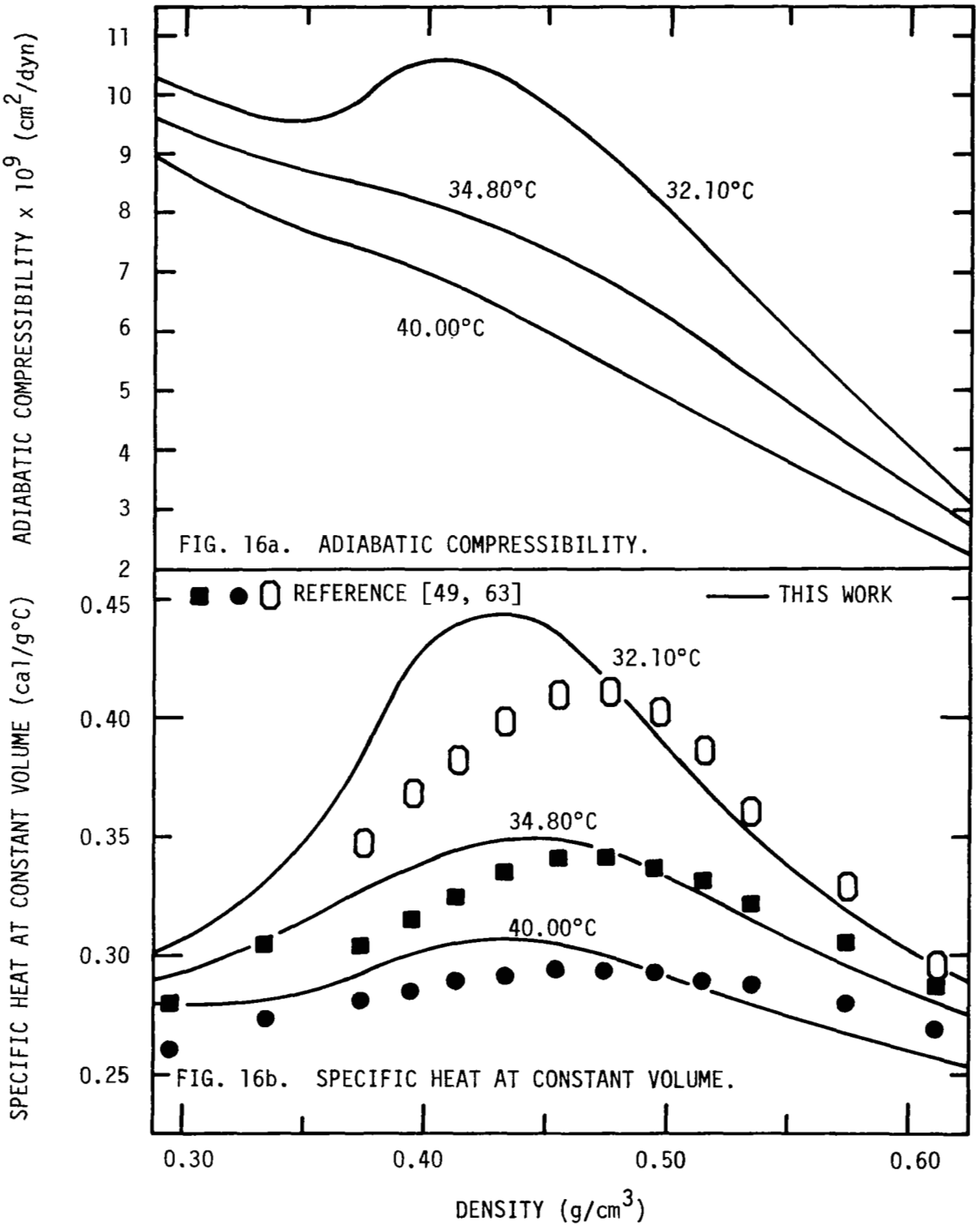

FIG. 16. ADIABATIC COMPRESSIBILITY AND SPECIFIC HEAT AT CONSTANT VOLUME AS A FUNCTION OF DENSITY IN CO_2.

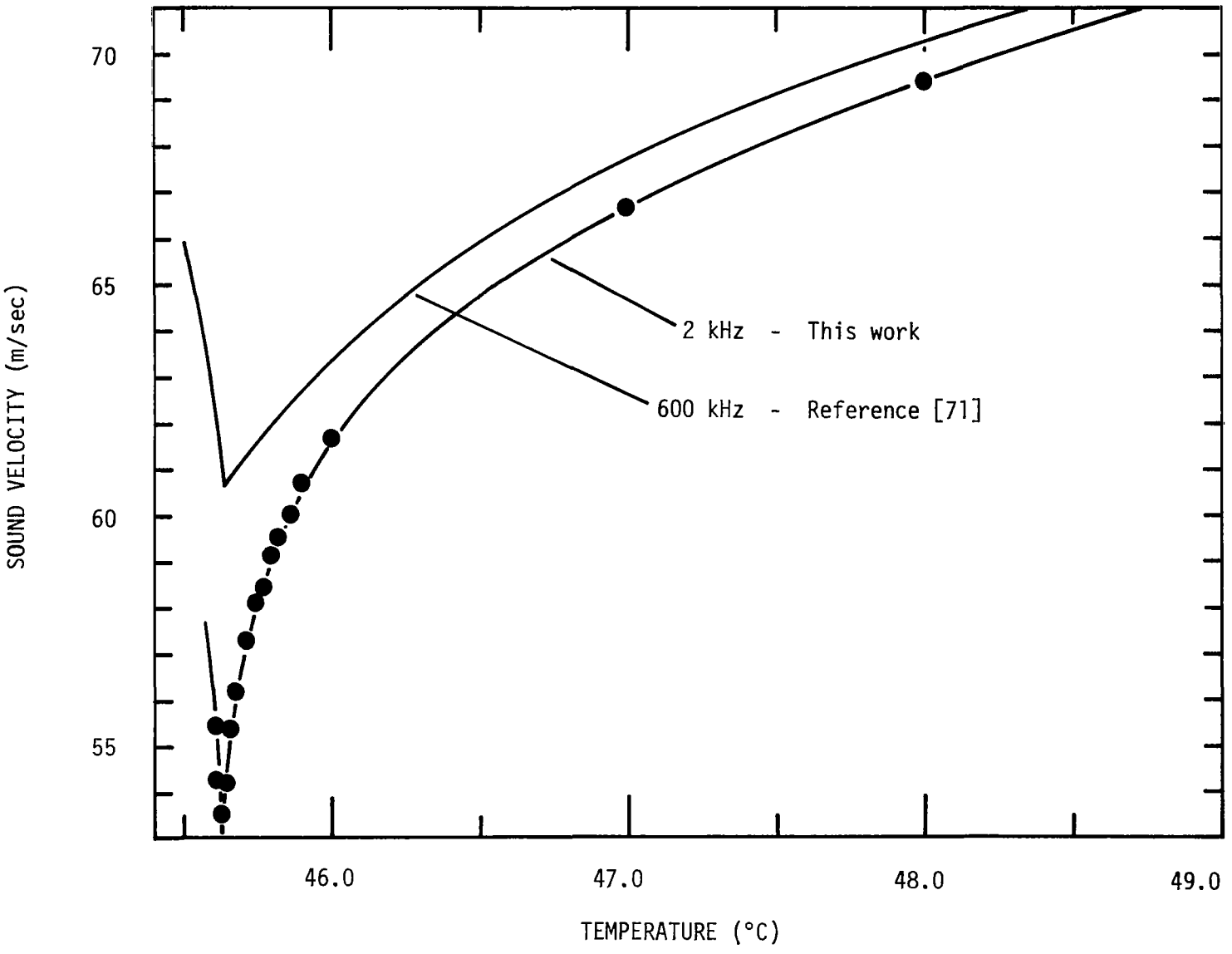

FIG. 17. SOUND VELOCITY AS A FUNCTION OF TEMPERATURE IN SF_6 AT CRITICAL DENSITY.

results we conclude that velocity dispersion does not occur up to this frequency except at very small values of $T-T_c$.

TABLE V Critical Parameters for SF_6

Reference	ρ_c (g/cm^3)	T_c (°C)	P_c (atm)
Clegg et al [50]	0.73-0.75	45.58	37.10
Wentorf [61]	0.725	45.64-45.68	37.20
MacCormack and Schneider [70]	0.73	45.547	37.11

This is in agreement with data obtained by Schneider at 600 kHz [71]. We have plotted his velocity values in Fig. 17 and these are only 1 m/sec higher than ours except very close to T_c. At T_c the difference is about 7 m/sec. It should be noted that Schneider's original paper [71] indicated values of velocity which were in error by a factor of 2. This was corrected in an Erratum [72]. Schneider reports that his temperature of meniscus disappearance, 45.65°C, coincided with the temperature of the minimum velocity in the vapor, liquid, and gas phases. This should be compared with our observation of the velocity minimum at 45.625°C. We should point out that our measurements discussed above agree very well with those we obtained using the condenser microphone type cells which for SF_6 resonated at approximately 500 Hz.

In Fig. 18 we have plotted κ_S as a function of $T-T_c$ for SF_6 as determined from these sound velocity values. We assumed $\rho = 0.70$ g/cm^3 for the computations. If one assumes logarithmic behavior at large values of $T-T_c$, then deviations from this behavior occur for $T-T_c<0.1$°C. From this we might conclude either that κ_S does not diverge or that the density gradient is more troublesome in SF_6 than in CO_2.

9.2 Acoustic Measurements in the Megahertz Region

9.2.1 Carbon Dioxide

Preliminary velocity and absorption measurements have been made in carbon dioxide at 1 MHz using the acoustic interferometric technique. Measurements were taken in the gaseous phase as the temperature was decreased to T_c. Since the absorption is very high in CO_2, the number of cavity length reso-

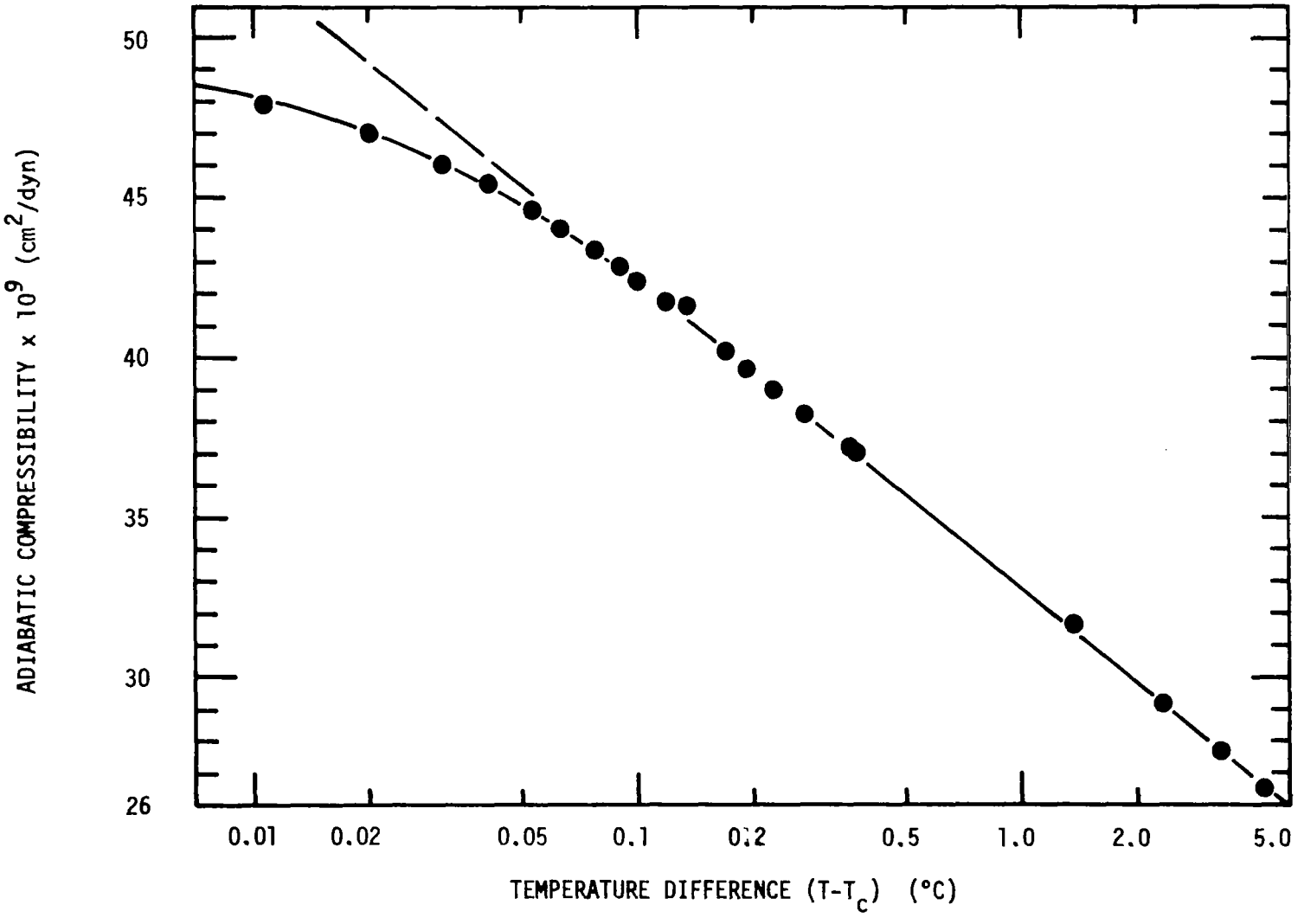

FIG. 18. ADIABATIC COMPRESSIBILITY AS A FUNCTION OF TEMPERATURE DIFFERENCE FOR SF_6 AT CRITICAL DENSITY.

nances detected decreased from about 50 at 40°C to 5 near the critical point. Thus the overall precision of this method also decreased as T approached T_c. For cells loaded to critical density velocities observed at 1 MHz agree within ±3% with those determined in the kilohertz region, except for $T-T_c<0.3$°C, when the kilohertz values become substantially lower. As already noted, the velocity minimum detected for $T\simeq T_c$ was 110 m/sec at 1 kHz while at 1 MHz the lowest values approached 130 m/sec. The difference may be due to velocity dispersion. However, further data should be taken with a redesigned fluid cell since the one used for the measurements reported here had an effective length of approximately 10 cm, although the acoustic cavity itself was much shorter. It was not possible to consistently fill the cell so that the small vertical segment where $\rho = \rho_c$ fell within the acoustic cavity. In addition, the sample purity for these measurements may be open to question since the velocity minima occurred at 31.25°C, i.e. substantially higher than in our kilohertz studies.

Our absorption measurements in CO_2 also have yielded only limited data. Initially we obtained data well away from the critical region to check our method. Measurements were made at 1 MHz and 50.6°C for densities ranging from 0.02 to 0.2 g/cm^3, corresponding to pressures from 7 to 80 atm, respectively. Our results in this range compare well with those reported by Henderson [59]. We then made measurements in the critical region. In Table VI we present typical results, obtained for a mean density ρ = 0.45 g/cm^3 in a run where we measured the absorption per wavelength $a\Lambda$ as a function of temperature as T approached T_c from above. Though the particular cell design used in this test leaves much to be desired we feel that these results are promising in that they indicate the method which may be used to obtain data quite close to the critical point.

TABLE VI Absorption per Wavelength in CO_2

T (°C)	$a\Lambda$ Dimensionless
40	.27
35	.12
32.2	.18
31.7	.29
31.537	.38
31.504	.41
31.480	.44
31.443	.46
31.378	.57
31.310	.69
31.253	.90
31.218	.42
31.203	.28

9.2.2 Sulfur Hexafluoride

We also obtained more extensive sound velocity and absorption data in sulfur hexafluoride at 1 MHz as a function of temperature at critical density. In Fig. 19 we present our velocity values obtained in the kilohertz and megahertz range as well as Schneider's earlier values [71]. In addition, we have included values in the hundred MHz region obtained with the light scattering technique. The latter will be discussed in the next section. It can be seen that our 1 MHz values lie slightly above those obtained by Schneider at 600 kHz and farther above the velocities we obtained in the kilohertz region. The only pronounced difference occurs at small values of $T-T_c$, where our low frequency measurements indicate a sharp decrease in velocity.

Data on the energy absorption per wavelength $a\Lambda$ is shown in Fig. 20. The solid lines represent values obtained by Schneider [71, 72] in the liquid and vapor phases. Our values agree qualitatively with his results but obviously our system must be improved to yield more accurate results. We can however, consider in some detail the behavior of $a\Lambda$ in the critical region. Schneider has pointed out that the large sound attenuation may be due either to sound scattering or to a relaxation process occuring in the critical region. In other experimental studies in progress in our laboratory on the behavior of binary liquid mixtures, it has been determined that sound scattering does not play a major role in the critical region. It seems reasonable to assume, for single component fluids in the critical region, that the large increase in $a\Lambda$ is due to an increase in the bulk viscosity. This might be interpreted in terms of the makeup and breakup of clusters of molecules during passage of a sound wave. If such a process becomes more out of phase with the driving force as the critical point is approached it would contribute to an increase in sound absorption. More precise absorption data is needed before one may determine the applicability of recent theoretical studies of such phenomena [35].

9.3 Light Scattering Measurements and Velocity Dispersion

We have carried out light scattering measurements in sulfur hexafluoride in the vapor phase and also in the gas phase above T_c, examining the spectrum of the Brillouin lines. Measurements were made at eight temperatures between 20 and 55°C, but no closer to T_c than 4°C. From the frequency shifts $\Delta\nu_B$ of the Brillouin lines we have determined the velocity of sound at a frequency of the order of 400 MHz. Our values agree well with those obtained by Ford et al (private communication) in a more detailed study, and these data are compared in Fig. 19. As yet we have not been able to obtain sufficient resolution of the scattered light spectra to be able to calculate the high frequency sound absorption coefficient from Brillouin line width measurements.

It is of interest to compare the high frequency sound velocities obtained by other workers in CO_2 [73] using light scattering techniques with the values we have measured using acoustic methods. These data are presented in Fig. 21. We have included values obtained acoustically in velocity versus pressure studies in the frequency range 0.2 to 2.0 MHz by various workers [73].

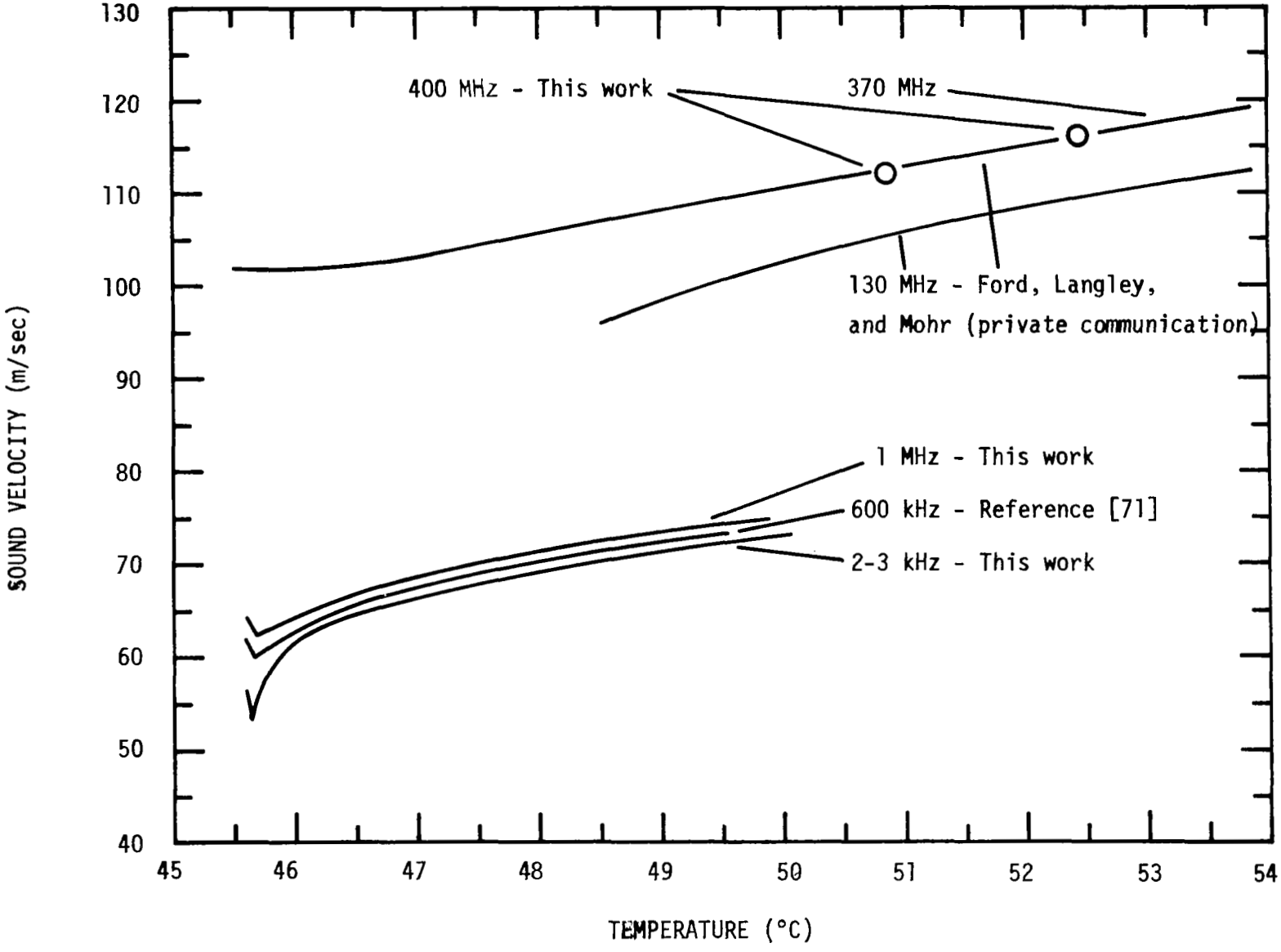

FIG. 19. SOUND VELOCITY AS A FUNCTION OF TEMPERATURE IN SF_6 AT CRITICAL DENSITY.

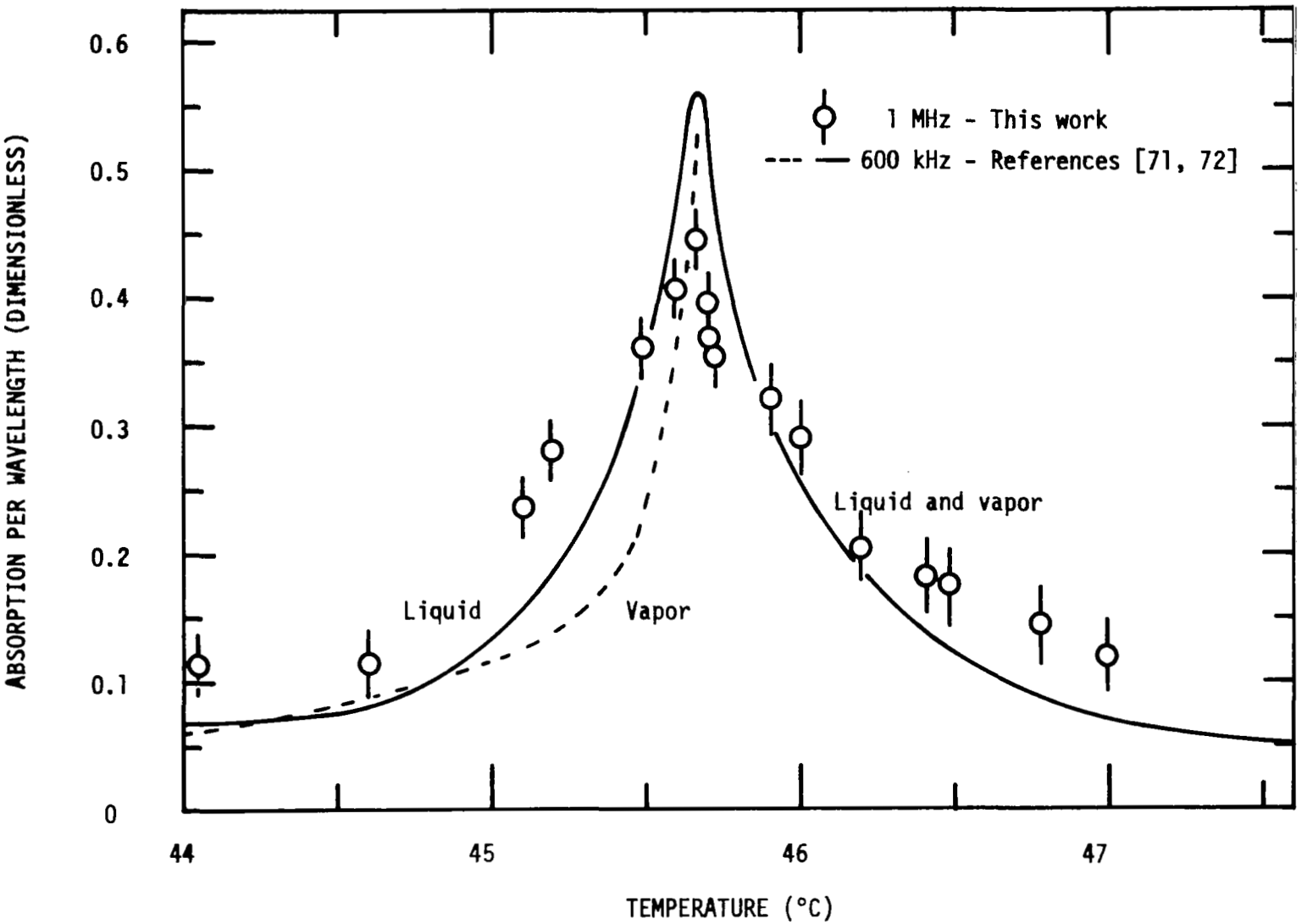

FIG. 20. SOUND ABSORPTION PER WAVELENGTH AS A FUNCTION OF TEMPERATURE IN SF_6.

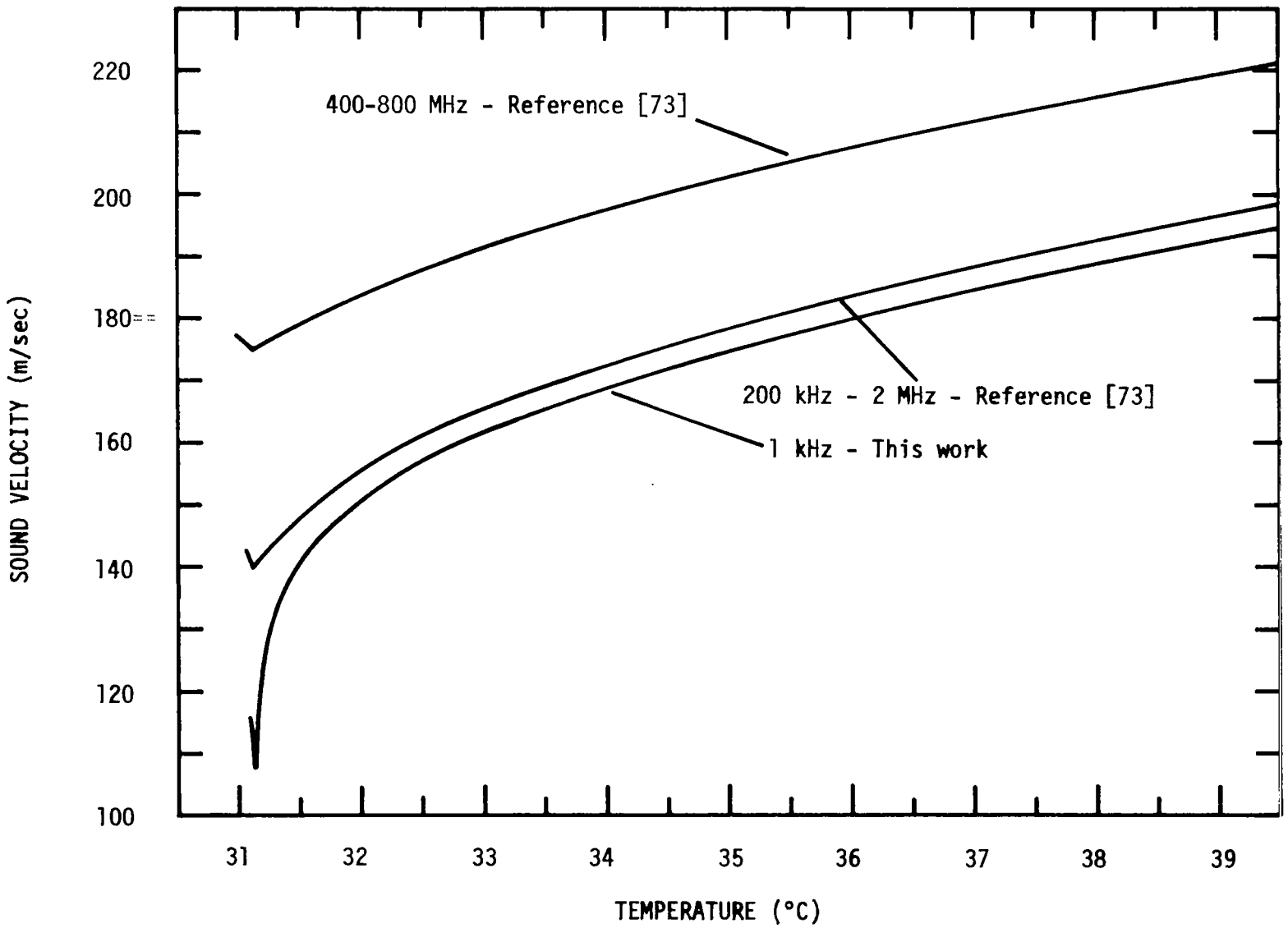

FIG. 21. SOUND VELOCITY AS A FUNCTION OF TEMPERATURE IN CO_2 AT CRITICAL DENSITY.

It is known that relaxation of the vibrational specific heat occurs in high density CO_2 in the low megahertz region [58, 59] and this accounts for much of the velocity dispersion noted at the larger values of $T-T_c$ [73]. As the critical region is approached, however, it appears from the velocity data that another form of relaxation process must become effective. Gammon et al [73] ascribed the additional velocity dispersion noted between the low megahertz values and their light scattering ones to a structural relaxation involving cluster formation and dissolution. The rather large disperison noted in our low frequency velocities, as indicated in Fig. 21 for $T-T_c<0.6°C$, further confirms such a conclusion.

X. CONCLUDING REMARKS

Much can be learned about the behavior of fluids in the vicinity of critical points by applying acoustic and light scattering techniques. During the past two years our group in the Physics Department of John Carroll University has developed precise methods for making measurements in fluids such as carbon dioxide and sulfur hexafluoride in the critical region. We have extended the range of applicability of acoustic and light scattering methods that we developed for earlier extensive studies of liquids. We now are able to accurately determine the velocity and absorption of sound in the frequency range from 1 kilohertz to several megahertz in the critical region. We also have perfected techniques for carrying out detailed light scattering studies.

From extensive data already obtained we have shown that it is feasible to take precise low frequency isochoric sound velocity measurements in single component fluids in the critical region. From such results we are able to determine the behavior of the adiabatic compressibility κ_S and the constant volume specific heat C_v as well as their critical exponents. We have concluded, subject to possible modifications that await satisfactory theoretical calculations of the effect of gravity induced density gradients, that in carbon dioxide κ_S has a logarithmic singularity for $\varepsilon = (T-T_c)/T_c < 3 \times 10^{-2}$ and for $T > T_c$ along the critical isochore. Furthermore, combining the results of our velocity measurements with available thermodynamic data we deduce that C_v may also be a logarithmically diverging function of $T-T_c$ for $\varepsilon < 3 \times 10^{-3}$, although behavior of the form $C_v \sim (T-T_c)^{-\alpha}$, with α small but not zero, cannot be ruled out if the region $\varepsilon < 2 \times 10^{-4}$ is considered separately. We have also obtained acoustic and light scattering data in sulfur hexafluoride. In the critical region density gradients appear to cause more severe problems in SF_6 than in CO_2 at comparable relative temperatures. Also necessary PVT data is not so readily available for SF_6. For these reasons further data will have to be obtained before definite conclusions may be drawn regarding its critical point behavior.

We plan to continue our acoustic and light scattering studies of fluids in the critical region. To improve our results we are modifying the temperature control systems used with our light scattering setups and are modifying our acoustic cells so that measurements may be taken on samples of smaller height to reduce errors associated with density gradients. We hope also to be able to obtain data on the sound absorption coefficient both at low frequencies where measurements of the frequency response of the resonant acoustic cavities now seem feasible and also from light scattering measurements by improving our systems for resolving the Brillouin lines.

APPENDIX A NOMENCLATURE

a	sound energy absorption coefficient
C	speed of light in vacuo
C_p	specific heat at constant pressure
C_v	specific heat at constant volume
C_{v_L} (C_{v_V})	specific heat at constant volume of the liquid (vapor) phase
F	Helmholtz free energy
g	gravitational acceleration
I_B	intensity of light scattered into one Brillouin line
I_R	intensity of light scattered into the Rayleigh line
$\vec{K}$	scattering wave vector
$\vec{k}_o$	wave vector of the incident light
$\vec{k}'$	wave vector of the scattered light
k_B	Boltzmann constant
ℓ	length of the resonant cavity
m	mass of fluid
n	refractive index
P	pressure
P_c	critical pressure
Q	heat
S	entropy
T	absolute temperature
T_c	critical temperature
u	sound velocity
u'	corrected sound velocity; see Eq. (49)
V	specific volume = $1/\rho$
V_c	critical specific volume
α,α',α''	critical exponents for the specific heat at constant volume
α_p	thermal expansion coefficient
β	critical exponent for the density difference between liquid and vapor phase
Γ	factor occurring in the sound absorption coefficient

Γ'	corrected Γ; see Eq. (48)
γ,γ'	critical exponents for the isothermal compressibility
γ^*	$= C_p/C_v$; ratio of specific heats
$\Delta\varepsilon$	deviation of the dielectric constant from its equilibrium value
$\Delta\nu_B(\Delta\nu_B')$	(corrected) linewidth of the Brillouin lines
$\Delta\nu_R(\Delta\nu_R')$	(corrected) linewidth of the Rayleight line
δ	critical exponent for the critical isotherm
ε	$= (T-T_c)/T_c$; relative temperature difference
ζ	bulk or volume viscosity
η	shear viscosity
Θ	scattering angle
κ_S	adiabatic compressibility
κ_T	isothermal compressibility
$\kappa_{T_L}(\kappa_{T_V})$	isothermal compressibility of the liquid (vapor) phase
Λ	acoustic wavelength
λ	wavelength of light
λ'	$= \Upsilon/(\rho C_p)$; thermal diffusivity
ν	frequency
ν_B	frequency shift of the Brillouin lines from the frequency of the incident light
ξ	long range correlation length
π	generalized critical exponent
ρ	mass density
ρ_c	critical mass density
ρ_L	mass density of the liquid
ρ_V	mass density of the vapor
τ_s	lifetime of the entropy fluctuations
Υ	thermal conductivity
Ω	molecular polarizability

REFERENCES

[1] Andrews, T., Phil. Trans. Roy. Soc. (London), vol. 159, 1869, p. 575.

[2] Onsager, L., "Crystal Statistics. I. A Two-Dimensional Model with an Order-Disorder Transition," Phys. Rev., vol. 65, nos. 3 & 4, February 1944, pp. 117-149.

[3] Widom, B., "Equation of State in the Neighborhood of the Critical Point," J. Chem. Phys., vol. 43, no. 11, December 1965, pp. 3898-3905.

[4] Griffiths, R.B., "Thermodynamic Functions for Fluids and Ferromagnets near the Critical Point," Phys. Rev., vol. 158, no. 1, June 1967, pp. 176-187.

[5] Kadanoff, L.P., Götze, W., Hamblen, D., Hecht, R., Lewis, E.A.S., Palciauskas, V.V., Rayl, M., Swift, J., Aspnes, D., and Kane, J., "Static Phenomena near Critical Points: Theory and Experiment," Rev. Mod. Phys., vol. 39, no. 2, April 1967, pp. 395-431.

[6] Fisher, M.E., "The Theory of Equilibrium Critical Phenomena," Reports on Progress in Physics, vol. 30, A.C. Stickland, ed., The Institute of Physics and the Physical Society, London, 1967, pp. 615-730.

[7] Critical Phenomena, Proceedings of a Conference held in Washington, D.C., April 1965, M.S. Green and J.V. Sengers, eds., National Bureau of Standards Miscellaneous Publication 273, U.S. Government Printing Office, Washington, D.C., issued December 1, 1966.

[8] Heller, P., "Experimental Investigations of Critical Phenomena," Reports on Progress in Physics, vol. 30, A.C. Stickland, ed., The Institute of Physics and the Physical Society, London, 1967, pp. 731-826.

[9] Voronel', A.V., Chashkin, Yu. R, Popov, V.A., and Simkin, V.G., "Measurement of the Specific Heat C_V of Oxygen near the Critical Point," Zh. Eksperim, i. Teor. Fiz., vol. 45, September 1963, pp. 828-830, [English transl.: Soviety Phys.-JETP, vol. 18, 1964, pp. 568-569].

[10] Voronel', A.V., Snigirev, V.G., and Chashkin, Yu. R., "Behavior of the Specific Heat C_V of Pure Substances near the Critical Point," Zh. Eksperim. i. Teor. Fiz., vol. 48, March 1965, pp. 981-984, [Eng. transl: Soviet Physics-JETP, vol. 21, no. 3, September 1965, pp. 653-655].

[11] Voronel', A.V., Zh. Fiz. Khimii, vol. 35, 1961, p. 958.

[12] Edwards, C., Lipa, T.A., and Buckingham, M.J., "Specific Heat of Xenon near the Critical Point," Phys. Rev. Letters, vol. 20, no. 10, March 1968, pp. 496-499.

[13] Moldover, M.R., and Little, W.A., "Specific Heat of He^3 and He^4 in the Neighborhood of Their Critical Points," Phys. Rev. Letters, vol. 15, no. 2, July 1965, pp. 54-56.

[14] Hirschfelder, J.O., Curtiss, C.F., and Bird, R. Byron, Molecular Theory of Gases and Liquids, M. Goeppert Mayer, advisory ed, John Wiley and Sons, New York, March 1964, p. 367.

[15] Lorentzen, H.L., "Studies of Critical Phenomena in Carbon Dioxide Contained in Vertical Tubes," Acta Chemica Scandinavica, vol. 7, no. 10, 1953, pp. 1335-1346.

[16] Michels, A., Levelt, J.M., and de Graaff, W., "Compressibility Isotherms of Argon at Temperatures between -25°C and -155°C, and at densities up to 640 Amagat (pressures up to 1050 Atmospheres)," Physica, vol. 24, 1958, pp. 659-671.

Michels, A., Levelt, J.M., and Wolkers, G.J., "Thermodynamic Properties of Argon at Temperatures between 0°C and -140°C and at densities up to 640 Amagat (pressures up to 1050 atm.)," ibid, pp. 769-794.

[17] Habgood, H.W., and Schneider, W.G., "PVT Measurements in the Critical Region of Xe," Can. J. Chem., vol. 32, 1954, pp. 98-112.

[18] Our reference [6], p. 705.

[19] Rushbrooke, G.S., and Wood, P.J., "On the High Temperature Staggered Susceptibility of Heisenberg Model Antiferromagnetics," Molec. Phys. vol. 6, no. 4, 1963, pp. 409-421.

[20] Sette, D., "Ultrasonic Investigation of Fluid System in the Neighborhood of Critical Points," our reference [7], pp. 183-196.

[21] Landau, L.D., and Lifshitz, E.M., Fluid Mechanics, Pergamon Press, London, 1959, p. 300.

[22] Sengers, J.V., "Transport Properties of Compressed Gases," Recent Advances in Engineering Science, vol. 3, A.C. Eringen, ed., Gordon and Breach, New York, 1968, pp. 153-196.

[23] Mountain, R.D., "Spectral Distribution of Scattered Light in a Simple Fluid," Rev. Mod. Phys., vol. 38, no. 1, January 1966, pp. 205-214.

[24] McIntyre, D., and Sengers, J.V., "Study of Fluids by Light Scattering," in Physics of Simple Fluids, Temperley, H.N.V., Rowlinson, J.S., and Rushbrooke, G.S., eds, North-Holland Publishing Company, Amsterdam, 1968, pp. 447-505.

[25] Einstein, A., "Theorie der Opaleszenz von homogenen Flüssigkeiten und Flüssigkeitsgemischen in der Nähe des kritischen Zustandes", Annalen der Physik, vol. 33, no. 16, 1910, pp. 1275-1298.

[26] Avenarius, M., "Ueberinnere Latente Wärme," Annalen der Physik, vol. 151, 1874, pp. 303-316.

[27] Ornstein, L.S., and Zernike, F., "Die linearen Dimensionen der Dichteschwankungen," Physikalische Zeitschrift, vol. 19, 1918, pp. 134-137.

Ornstein, L.S., and Zernike, F., "Bemerkung zur Arbeit von Herrn K.C. Kar: Die Molekular zerstreuung des Lichtes beim kritischen Zustande," ibid, vol. 27, 1926, pp. 761-763.

[28] Landau, L., and Placzek, G., "Struktur der unverschobenen Streulinie," Physikalische Zeitschrift der Sowjetunion, vol. 5, 1934, pp. 172-173.

[29]. Ford, N.C., Jr., and Benedek, G.B., "The Spectrum of Light Inelastically Scattered by a Fluid near its Critical Point", Reference [7], pp. 150-156.

Ford, N.C., Jr., and Benedek, G.B., "Observation of the Spectrum of Light Scattered from a Pure Fluid near its Critical Point," Phys. Rev. Letters, vol. 15, no. 16, October 1965, pp. 649-653.

[30] Brillouin, L. "Diffusion de la lumiere par un corps transparent homogene," Academie des Sciences, Comptes Rendus, vol. 158, May 1914, pp. 1331-1334.

Brillouin, L., "Diffusion de la lumiere et des Rayons X par un corps transparent homogene - Influence de l'agitation thermique," Annales de Physique, vol. 17, 1922, pp. 88-122

[31] Mountain, R.D., "Thermal Relaxation and Brillouin Scattering in Liquids," J. of Research of the National Bureau of Standards, vol. 70A, no. 3, May-June 1966, pp. 207-220.

[32] Montrose, C.J., Solovyev, V.A., and Litovitz, T.A., "Brillouin Scattering and Relaxation in Liquids," J. Acoust. Soc. Am., vol. 43, no. 1, January 1968, pp. 117-130.

[33] Nichols, W.H., and Carome,E.F., "Light Scattering from a Multiply Relaxing Fluid", J. Chem. Phys., vol. 49, no. 3, August 1968, pp. 1000-1012.

[34] Our reference [23], p. 213.

[35] Kadanoff, L.P., and Swift, J., "Transport Coefficients near the Critical Point: A Master-Equation Approach", Phys. Rev., vol. 165, no. 1, January 1968, pp. 310-322.

"Transport Coefficients near the Liquid-Gas Critical Point," Phys. Rev. vol. 166, no. 1, February 1968, pp. 89-101.

[36] Ford, N.C., Jr., Langley, K.H., and Puglielli, V.G.,"Brillouin Linewidths in CO_2 near the Critical Point", Phys. Rev. Letters, vol. 21, no. 1, July 1968, pp. 9-12.

[37] Fixman, M., "Density Correlations, Critical Opalescence, and the Free Energy of Nonuniform Fluids," J. Chem. Phys., vol. 33, no. 5, November 1960, pp. 1357-1362.

Fixman, M., "Ultrasonic Attenuation in the Critical Region," ibid, pp. 1363-1370.

[38] Botch, W.D., "Studies of Some Critical Phenomena," thesis (Ph.D.), University of Oregon, 1963.

Botch, W., and Fixman, M., "Sound Absorption in Gases in the Critical Region," J. Chem. Phys., vol. 42, no. 1, January 1965, pp. 199-204.

[39] Lorentzen, H.L., "Studies of Critical Phenomena in Carbon Dioxide Contained in Vertical Tubes," Acta Chemica Scandiavica, vol. 7, no. 10, 1953, pp. 1335-1346.

[40] Schmidt, E.H.W., "Optical Measurements of the Density Gradients Produced by Gravity in CO_2, N_2O, and $CClF_3$ near the Critical Point," reference [7], pp. 13-20.

[41] Our reference [8], p. 745-746.

[42] vanDael, W., van Itterbeek, A., and Thoen, J., in Advances in Cryogenic Engineering, vol. 12, K.D. Timmerhaus, ed., Plenum Press, New York, 1967, p. 754.

[43] Ahlers, G., "Thermodynamics of the Isentropic Sound Velocity near the Superfluid Transition in He^4," Phys. Rev., vol. 182, no. 1, June 1969, pp. 352-362.

[44] Schmidt, E.H.W., and Traube, K., Progress in International Research on Thermodynamic and Transport Properties, American Society of Mechanical Engineers, New York, 1962, p. 193.

[45] Larsen, S.Y., Mountain, R.D., and Zwanzig, R., "On the Validity of the Lorentz-Lorenz Equation near the Critical Point," J. Chem. Phys., vol. 42, no. 6, March 1965, pp. 2187-2190.

[46] Morse, P.M., Vibration and Sound, 2nd edition, McGraw-Hill, New York, 1948, pp. 397-401.

[47] Pierce, G.W., "Piezoelectric Crystal Oscillators Applied to the Precision Measurements of the Velocity of Sound in Air and CO_2 at High Frequencies," Proc. Am. Acad. of Arts and Sciences, vol. 60, October 1925, pp. 269-302.

[48] Hubbard, J.C., "The Acoustic Resonator Interferometer: I. The Acoustic System and its Equivalent Electric Network," Phys. Rev., vol. 38, September 1931, pp. 1011-1019.

Hubbard, J.C., "The Acoustic Resonance Interferometer: II. Ultrasonic Velocity and Absorption in Gases," Phys. Rev., vol. 41, August 1932, pp. 523-535.

[49] The PVT and thermodynamic derivative data for CO_2 were compiled by Dr. J.V. Sengers from experiments of the van der Waals laboratory. The sources of data are given in Refs. 45-51 of our reference [23].

[50] Clegg, H.P., Rowlinson, J.S., and Sutton, J.R., "The Physical Properties of Some Fluorine Compounds and Their Solutions. Part I - Sulphur Hexafluoride," Trans. Faraday Soc., vol. 51, 1955, pp. 1327-1333.

[51] Mears, W.H., Rosenthal, E., and Sinka, J.V., "Physical Properties and Virial Coefficients of Sulfur Hexafluoride," J. Phys. Chem., vol. 73, no. 7, July 1969, pp. 2254-2261.

[52] Carome, E.F., Gutowski, F.A., and Schuele, D.E., "Basic Concepts of Ultrasonic Interferometry in Liquids," Am. J. of Physics, vol. 25, no. 8, November 1957, pp. 556-564.

[53] Fritsch, K., "A Study of Relaxation in Electrolytic Solutions using Ultrasonic and Laser Light Scattering Techniques," thesis (Ph.D.) 1968, The Catholic University of America, (Available from University Microfilms, Inc.,Ann Arbor, Michigan, #69-8871).

[54] Eberhardt, E.H., "Multiplier Phototubes for Single-Electron Counting," Electrical Communication, vol. 40, no. 1, 1965, pp. 124-133.

[55] Eberhardt, E.H., "Multiplier Phototubes as Quantum Counters," Applied Optics, vol. 6, no. 1, January 1967, pp. 161-162.

[56] ITT Industrial Laboratories, Fort Wayne, Indiana, Application Note E5, "Single Photon-Electron Counting With Multiplier Phototubes."

[57] Born, M. and Wolf, E., Principles of Optics, Second edition, Pergamon Press, Oxford, 1964, pp. 329-341.

[58] Henderson, M.C., and Peselnick, L., "Ultrasonic Velocity and Thermal Relaxation in Dry CO_2 at Moderate Pressures," J. Acoust. Soc. Am., vol. 29, no. 10, October 1957, pp. 1074-1080.

[59] Henderson, M.C., and Klose, J.Z., "Ultrasonic Absorption and Thermal Relaxation in CO_2," J. Acoust. Soc. Am., vol. 31, no. 1, January 1959, pp. 29-33.

[60] Michels, A., Blaisse, B., and Michels, C., "The Isotherms of CO_2 in the Neighbourhood of the Critical Point and Round the Coexistence Line," Proc. Roy. Soc. (London), vol. A160, 1937, pp. 358-375.

[61] Wentorf, R.H., "Isotherms in the Critical Regions of Carbon Dioxide and Sulfur Hexafluoride," J. Chem. Phys., vol. 24, no. 3, March 1956, pp. 607-615.

[62] Swinney, H.L., "The Spectrum of Light Scattered by Carbon Dioxide in the Critical Region," thesis (Ph.D.) 1968, The Johns Hopkins University (Available from University Microfilms, Inc., Ann Arbor, Michigan, #68-16,487).

[63] Michels, A., and Strijland, J., "The Specific Heat at Constant Volume of Compressed Carbon Dioxide," Physica, vol. 18, no. 8-9, August-September 1952, pp. 613-628.

[64] Williamson, R.C., and Chase C.E., "Velocity of Sound at 1 MHz near the He^4 Critical Point," Phys. Rev., vol. 176, no. 1, December 1968, pp. 285-294.

[65] Herget, C.M., "Ultrasonic Velocity in Carbon Dioxide and Ethylene in the Critical Region", J. Chem. Phys., vol. 8, July 1940, pp. 537-542.

[66] Anderson, N.S. and Delsasso, L.P., "The Propagation of Sound in Carbon Dioxide near the Critical Point", J. Acoust. Soc. Am., vol. 23, no. 4, July 1951, pp. 423-429.

[67] Tielsch, H., and Tanneberger, H., "Ultraschallausbreitung in Kohlensäure in der Nähe des kritischen Punktes," Zeits. für Physik, vol. 137, 1954, pp. 256-264.

[68] Trelin, Yu. S., and Sheludyakov, E.P. "Experimental Determination of the Speed of Sound in the Critical Region of Carbon Dioxide," Zh. Eksperim. i. Teor. Fiz., vol. 3, no. 2, January 1966, pp. 101-103 [Eng. transl.: Soviet Physics-JETP Letters, vol. 3,1966, pp. 63-64].

[69] Bagatskii, M.I., Voronel', A.V., and Gusak, V.G., "Measurement of the Specific Heat C_V of Argon in the Immediate Vicinity of the Critical Point", Zh, Eksperim. i. Teor. Fiz., vol. 43, August 1962, pp. 728-729 [Eng. transl.: Soviet Physics-JETP, vol. 16, no. 2, February 1963, pp. 517-518].

[70] MacCormack, K.E., and Schneider, W.G., "Isotherms of Sulphur Hexafluoride in the Critical Temperature Region, Can. J. Chem., vol. 29, 1951, pp. 699-714.

[71] Schneider, W.G., "Ultrasonic Absorption in the Critical Temperature Region," J. Chem. Phys., vol. 18, 1950, p. 1300.

Schneider, W.G., "Sound Velocity and Sound Absorption in the Critical Temperature Region," Can. J. Chem., vol. 29, 1951, pp. 243-252.

[72] Schneider, W.G., "Erratum: Ultrasonic Absorption in the Critical Temperature Region", J. Chem. Phys., vol. 20, 1952, pp. 759-760.

[73] Gammon, R.W., Swinney, H.L., and Cummins, H.Z., "Brillouin Scattering in Carbon Dioxide in the Critical Region", Phys. Rev. Letters, vol. 19, no. 26, December 1967, pp. 1467-1469.

NASA-Langley, 1970 —— 33 E-5714